

AN ABSTRACT OF THE THESIS OF

Andrew Heath Barnard for the degree of Master of Science in
Oceanography presented on August 19, 1993.

Title: Seasonal Variability of Zooplankton off the California Coast: A Box Model Approach.

Redacted for Privacy

Abstract Approved:


Dudley B. Chelton

In an effort to elucidate the mechanism responsible for large-scale zooplankton variability in the California Current, zooplankton biomass and hydrographic data from the California Cooperative Fisheries Investigation data set and wind data from Fleet Numerical Oceanography Center model analyses have been used to construct a box model biomass budget. The box model method was implemented to examine the effects of advection on determining the observed seasonal variability of zooplankton biomass in the California Current system. The box model utilizes the monthly sampled data for the years 1950-1982 to construct seasonal cycles of zooplankton biomass and current velocity from which the advective component of seasonal biomass variability can be estimated. Current velocities in the box model included both the geostrophic and Ekman transport components in the upper surface layer.

The results of the model indicate that, while large-scale advection of zooplankton in the California Current is strong, it clearly is not the sole controlling mechanism of the observed seasonal variability in zooplankton biomass. It is concluded that meso-scale features and local zooplankton growth/loss processes, which cannot be resolved by the CalCOFI data set, are more important in determining the seasonal cycles of zooplankton biomass in the California Current system than has previously been recognized.

Seasonal Variability of Zooplankton off
the California Coast: A Box Model
Approach.

by

Andrew Heath Barnard

A THESIS

submitted to

Oregon State University

in partial fulfillment of
the requirements for the
degree of

Master of Science

Completed August 19, 1993

Commencement June 1994

APPROVED:

Redacted for Privacy

Professor of Oceanography in charge of major

Redacted for Privacy

Head of department of Oceanography

Redacted for Privacy

Dean of Graduate School

Date thesis is presented August 19, 1993
Typed by researcher for Andrew Heath Barnard

ACKNOWLEDGMENTS

I would like to thank the entire CalCOFI sampling group for providing the oceanographic research community with an extensive and unique data set. Special thanks go to Paul E. Smith at the National Marine Fisheries Service in La Jolla, California for supplying the comprehensive CalCOFI zooplankton data, and to Larry Eber for providing the hydrographic data. I would also like to thank Don Vanderpool at Goddard National Space Data Center in Greenbelt, Maryland for providing the FNOG marine surface wind data.

I would like to recognize my thesis advisor, Dudley Chelton, whose scientific guidance, personal insight and careful reviews of the manuscript were invaluable to my progression as a scientist. Special thanks go to Leonard Walstad for helping me to understand the basics of biophysical modeling. Thanks to Mark Abbott and Tim Cowles for helping me to bridge the gap between the biology and physics of the model. Thanks to Mark for his financial support. This work was also supported by a NASA Global Change Fellowship.

I am indebted to Donna Witter, Collin Roesler and Mary-Elena Carr for their constructive comments on earlier versions of this manuscript and for their emotional support. I would also like to thank my friends Dylan Righi, Naara Johnson, Sue Ross, Lynne Fessenden and Joe Ortiz who were always supportive during my successes and set backs. Peter Franks merits special attention for his assistance in the development of the model and for his constructive comments on my NASA Global Change Fellowship Proposal.

Most of all I would like to thank my wife, Lisal, without whom I couldn't have finished. Her patience and encouragement have been the guiding light throughout my graduate career. This thesis is dedicated to her and to my parents for providing me with the drive to continually challenge myself.

TABLE OF CONTENTS

	<u>Page</u>
INTRODUCTION	1
DATA DESCRIPTION AND METHODS	13
1. CalCOFI Data Description	13
2. FNOG Wind Data Description	17
3. Region Descriptions	17
4. Derivation of Box Model Equations	19
5. Computational Details	25
6. Estimating Local Zooplankton Growth/Loss	29
RESULTS	32
1. Large-scale Seasonal Patterns	33
2. Geostrophic versus Ekman Zooplankton Transport	39
3. Net Advection and Observed Zooplankton Productivity	42
4. Zooplankton Productivity from Local Biological Processes	55
5. Zooplankton Seasonal Cycles	58
DISCUSSION	64
SUMMARY	71
REFERENCES	73
APPENDICES	
APPENDIX A: Box Model Assumptions	77
APPENDIX B: Interpolations of Zooplankton and Dynamic Height Data	84
APPENDIX C: The Appearance and Removal of Secular Terms	88

LIST OF TABLES

<u>Table</u>	<u>Page</u>
1. Horizontal dimensions and volume of each box model region.	18
2. Estimates of local zooplankton growth rates. Temperature-based growth rates were calculated using Huntley and Lopez (1992) model of zooplankton growth. Sea surface temperature ranges were determined from CalCOFI measurements as the average temperatures observed in each region during spring. Model estimates of growth rates were obtained from Figures 15-18, panel b as the maximum positive slope.	69

LIST OF FIGURES

<u>Figure</u>	<u>Page</u>
1. Geographical location of the 23 areal averaged zooplankton data points from CalCOFI samples (provided by Paul E. Smith). The fourteen regions found to have ample observations to determine the seasonal cycle by harmonic regression are bordered by solid lines. Also shown are the locations of the four areal averaged areas (bold lines) used by Roesler and Chelton (1987) and Chelton et al. (1982) in the study of non-seasonal zooplankton and large-scale advection. Taken from Roesler and Chelton, (1987), their Figure 4.	5
2. Comparison of the seasonal cycles of zooplankton displacement volume and alongshore geostrophic flow in the 14 regions used by Roesler and Chelton (1987), their Figure 6.	7
3. CalCOFI geographic sampling grid indication line and station locations. Taken from CalCOFI Reports (1988).	14
4. CalCOFI zooplankton and dynamic height as well as FNOG marine surface winds data point locations used in this study. Also shown are the geographical locations of the four box model study areas labeled 1, 2, 3 and 4.	16
5. Contour maps of zooplankton displacement volume using the 32 year record of the 14 areal averaged zooplankton data points regressed to an annual and semiannual seasonal cycle (plus a constant offset) interpolated to a fine mesh grid. Contour interval is 0.1 ml/1000 L.	34
6. Contour maps of 0/500 db dynamic height using the full 32 year record of the 149 dynamic height data points regressed to an annual and semiannual seasonal cycle (plus a constant offset) interpolated to a fine mesh grid. Contour interval is 0.08 m.	35
7. Seasonal pattern of wind stress obtained from harmonic regressions of the 36 FNOG marine surface data points and interpolated to a fine mesh grid. 1 inch = 0.4 N/m ² .	37
8. Ekman transport averaged by season. Obtained using the interpolated wind stress values on the fine mesh grid. 1 inch = 4 m ² /day.	38
9. Time series of net geostrophic (solid lines) and net Ekman (dashed lines) zooplankton transport obtained in each of the four model regions.	40

<u>Figure</u>	<u>Page</u>
10. For region 1, <i>a</i> , the time series of alongshore gradient in observed zooplankton biomass, shown as a solid line, calculated as the difference between the north and south face average zooplankton concentration. The time series cross-shore gradient in observed zooplankton biomass, shown as a dashed line, is calculated as the difference of the east and west face average zooplankton concentrations. <i>b</i> , time series of advective transport of zooplankton through the surface area of the north (solid line), south (thick solid line), west (dashed line) and east (thick dashed line) faces of region 1. Positive values indicate transport into the region, while negative values indicate transport of zooplankton out of the region. <i>c</i> , time series of alongshore divergence in zooplankton biomass transport, shown as a solid line, calculated as the sum of the north and south face advective transport of zooplankton. The cross-shore divergence of zooplankton, calculated as the sum of the east and west face transports, is shown as a dashed line. Note that these time series have been normalized by the volume of region 1. <i>d</i> , time series of the observed change in zooplankton biomass over the volume of region 1 (solid line) and the time series of the net advection of zooplankton through region 1 (dashed line).	44
11. Same as Figure 10, for region 2.	48
12. Same as Figure 10, for region 3.	50
13. Same as Figure 10, for region 4.	53
14. The difference between the change in the observed zooplankton biomass and the net advection of zooplankton time series, shown in Figures 10-13, panel d, for each of the four model study regions. The difference time series for region 1 is drawn as a solid line, region 2 as a dashed line, region 3 as a thick solid line and region 4 as a thick dashed line.	56
15. For region 1, <i>a</i> , seasonal cycles of the volume integral of observed zooplankton biomass (solid line) and advected zooplankton biomass (thick solid line) in region 1. Also plotted is the seasonal mean of the observed zooplankton biomass as a dashed line. <i>b</i> , difference between the observed and advected zooplankton time series shown in panel a, representing the seasonal cycle of local zooplankton biomass.	59
16. Same as Figure 15, for region 2.	60
17. Same as Figure 15, for region 3.	61

<u>Figure</u>	<u>Page</u>
18. Same as Figure 15, for region 4.	62
19. Seasonal cycles of wind-driven upwelling velocity averaged over each of the four regions. Region 1 is plotted as a solid line, region 2 as a dashed line, region 3 as a thick solid line and region 4 as a thick dashed line.	81
20. Root mean square error obtained from interpolations of varying wavelength analytical data using the 14 zooplankton grid point locations used in this study.	85
21. Same as Figure 20, using the 149 dynamic height grid point locations.	87

Seasonal Variability of Zooplankton off the California Coast:
A Box Model Approach

INTRODUCTION

Eastern boundary current ecosystems have long been recognized as some of the most biologically productive areas of the world ocean (Reid, 1962; Ryther, 1969). These ecosystems are complex, often having multiple mass and chemical energy inputs which can be channeled directly into organic production. In addition, eastern boundary current ecosystems are also open to inputs of mechanical energy in the form of advection and local wind forcing which may have indirect effects on organic production. The question of how the physical and biological dynamics in these regions interact in relation to production remains unsolved. The objective of the present study is to examine the effects of advection on the seasonal biological structure of the California Current eastern boundary ecosystem. In particular, is seasonal variability in the observed zooplankton biomass due to variations in large-scale advection of zooplankton biomass from the north?

The California Current system, the eastern limb of the North Pacific gyre, is comprised of a broad surficial current (California Current) flowing along the coast of the United States and Baja California, and a poleward undercurrent (California Undercurrent) concentrated over the continental slope. The California Current flows equatorward year round and is relatively

shallow in depth (0-300m). Maximum velocities occur at or near the surface. Typical flow speeds are 4 to 10 cm/sec (Reid and Schwartzlose, 1962). The western extent of the California Current lies approximately 850 to 900 km off the California coast (Lynn and Simpson, 1987).

Off central California, the core of the equatorward California Current occurs 100 to 200 km offshore, with strongest velocities occurring in February-March and again in July-August (Chelton, 1984). The poleward California Undercurrent (CU), which underlies the California Current, generally does not extend more than 150 km from the coast. Strong poleward flow occurs at the surface during fall and winter and is confined to the continental slope region within 75-100 km of the coast (Hickey, 1979; Chelton, 1984). This surficial poleward flow is often referred to as the Inshore Countercurrent. North of Point Conception, it is more commonly known as the Davidson Current.

Off southern California, two maxima in the equatorward flow are apparent. One occurs approximately 250 km offshore during the summer and the other is in midwinter 180 km farther west (Lynn and Simpson, 1987). In the early summer, the California Current branches off, forming shoreward and southward components as it moves south of Point Conception. The shoreward component of this flow defines the southern edge of a cyclonic eddy which is geographically fixed about the shallow offshore banks of the Southern California Bight. Near the coast, poleward flow is observed during summer through fall due to flow around the cyclonic eddy (Simpson, et al., 1984). The southern component of the California Current draws near the coast as it flows along Baja California, bending westward slightly as it moves around

Punta Eugenia at about 27.5° N. Maximum equatorward velocities off Baja California are observed in spring (Hickey, 1979).

The surface water properties of the California Current are defined by Alaskan Subarctic gyre, North Pacific Central gyre, and coastal upwelled waters. Of particular interest to this study is the Alaskan Subarctic gyre water, which forms the bulk of the source waters of the California Current (Hickey, 1979). This water mass is characterized by low temperature, low salinity, high nutrients and high zooplankton biomass (Reid, 1962). North Pacific Central gyre waters are characterized by high temperature and salinity and low nutrients and biomass. Coastal upwelled water is generally restricted to nearshore regions (<100 km offshore), and is characterized by low temperatures, high salinities and high nutrient concentrations. The differences in water properties between these three sources may allow the biological impact of each within the ecosystem of the California Current to be assessed.

Using salinity maps constructed by the NORPAC Committee (1960) for July through September, Roesler and Chelton (1987) traced the subarctic water mass as a large-scale tongue extending from the subarctic gyre equatorward to about 25° latitude from the surface to depths shallower than 200 m. Lynn and Simpson (1987) calculated salinity on a surface of constant density and found that low salinities, similar to the subarctic water mass, could be traced equatorward from the subarctic Pacific to southern Baja California during the period of strong southerly flow. Clearly the biology of the California Current system may be dramatically influenced by the variations in the equatorward flow of this high-nutrient, high-biomass water mass.

A correlation between zooplankton biomass and advection has been suggested in many previous studies of the California Current. Reid (1962) found an inverse relationship between surface temperature and zooplankton biomass. He suggested that the equatorward movement of the California Current advected cold, nutrient- and biomass-rich waters southward along the coast. From the 1955-59 California Cooperative Oceanic Fisheries Investigations (CalCOFI) zooplankton biomass data set, Colebrook (1977) found that specific zooplankton taxa were highly coherent with the general variability in zooplankton biomass. He suggested that the large-scale variability is a result of a physical process rather than a local interaction, and that the source of this variability must either originate in the northern portion of the California Current or affect the northern populations to a greater degree.

Studies by Hemingway (1976), Bernal (1981), Bernal and McGowan (1981) and Chelton et al. (1982) in the California Current suggested that variations in primary production, driven by the advection of nutrients from the north, cause a local response in the zooplankton biomass. Chelton et al. also noted that, even though the northern species of zooplankton are found in the southern portions of the California Current, they never appear to dominate. This suggests that a simple passive advection mechanism cannot fully explain the observed variability in zooplankton. However, the spatial resolution used in that study was extremely coarse as the zooplankton biomass data were pooled into 4 areal averages (Figure 1).

Two mechanisms have been postulated to explain the seasonal zooplankton biomass variability; (1) passive advection of zooplankton from the

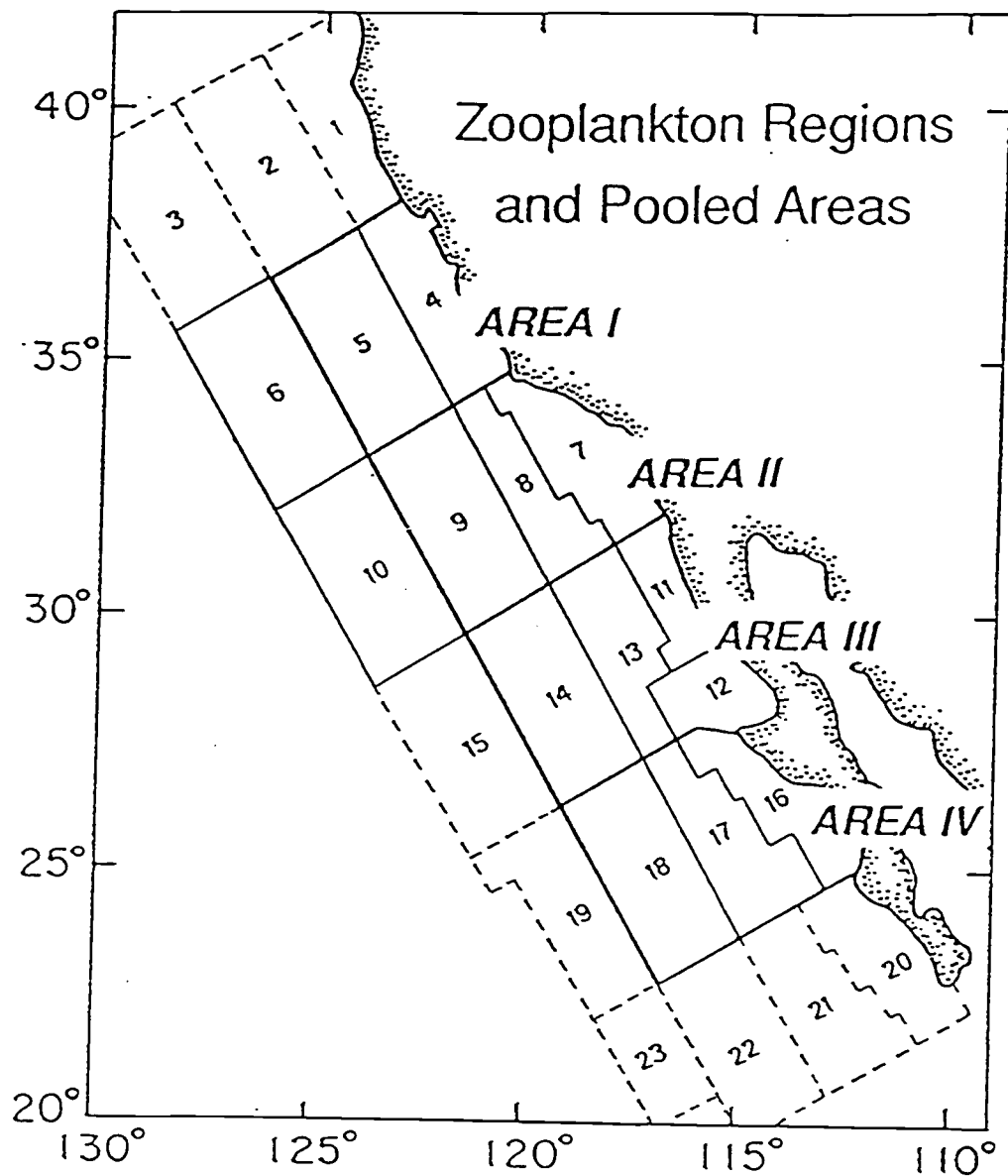


Figure 1 - Geographical location of the 23 areal averaged zooplankton data points from CalCOFI samples (provided by Paul E. Smith). The fourteen regions found to have ample observations to determine the seasonal cycle by harmonic regression are bordered by solid lines. Also shown are the locations of the four areal averaged areas (bold lines) used by Roesler and Chelton (1987) and Chelton et al. (1982) in the study of nonseasonal zooplankton and large-scale advection. Taken from Roesler and Chelton, (1987), their Figure 4.

north and (2) a local response in zooplankton (via primary production) due to the influx of nutrients and/or phytoplankton by vertical and horizontal advection. The key to differentiating between these two processes may be in the time scale of each process. In the passive advection scenario, an almost instantaneous response (~1 month) in the time rate of change in zooplankton biomass should be observed in correspondence with advection from the north. Because of the time required for intermediate biological processes (i.e., primary production), a longer time lag is expected between advection from the north and the time rate of change in zooplankton biomass in the nutrient advection scenario. In areas of weak flow, this time scale has been estimated to be 3-5 months (Raymont 1980, Walsh 1977).

Roesler and Chelton (1987) attempted to assess the relative importance of these two hypotheses on seasonal and interannual time scales using hydrographic and zooplankton CalCOFI data from 1950-82. The zooplankton data were pooled into 23 areal averages, of which 14 were determined to have sufficient data to determine the seasonal cycles (Figure 1). Over the seasonal cycle, they found a strong similarity between the amplitudes and phases of maxima/minima in geostrophic flow and maxima/minima in zooplankton biomass (Figure 2). Based on these observations, they concluded that the seasonal variability in the large-scale zooplankton biomass is dominated by passive alongshore geostrophic advection. However, Roesler and Chelton did not consider the cross-shore component of flow, which can contribute significantly to fluctuations in zooplankton biomass. Furthermore, the seasonal cycle of zooplankton biomass should be 90° out of phase with the time

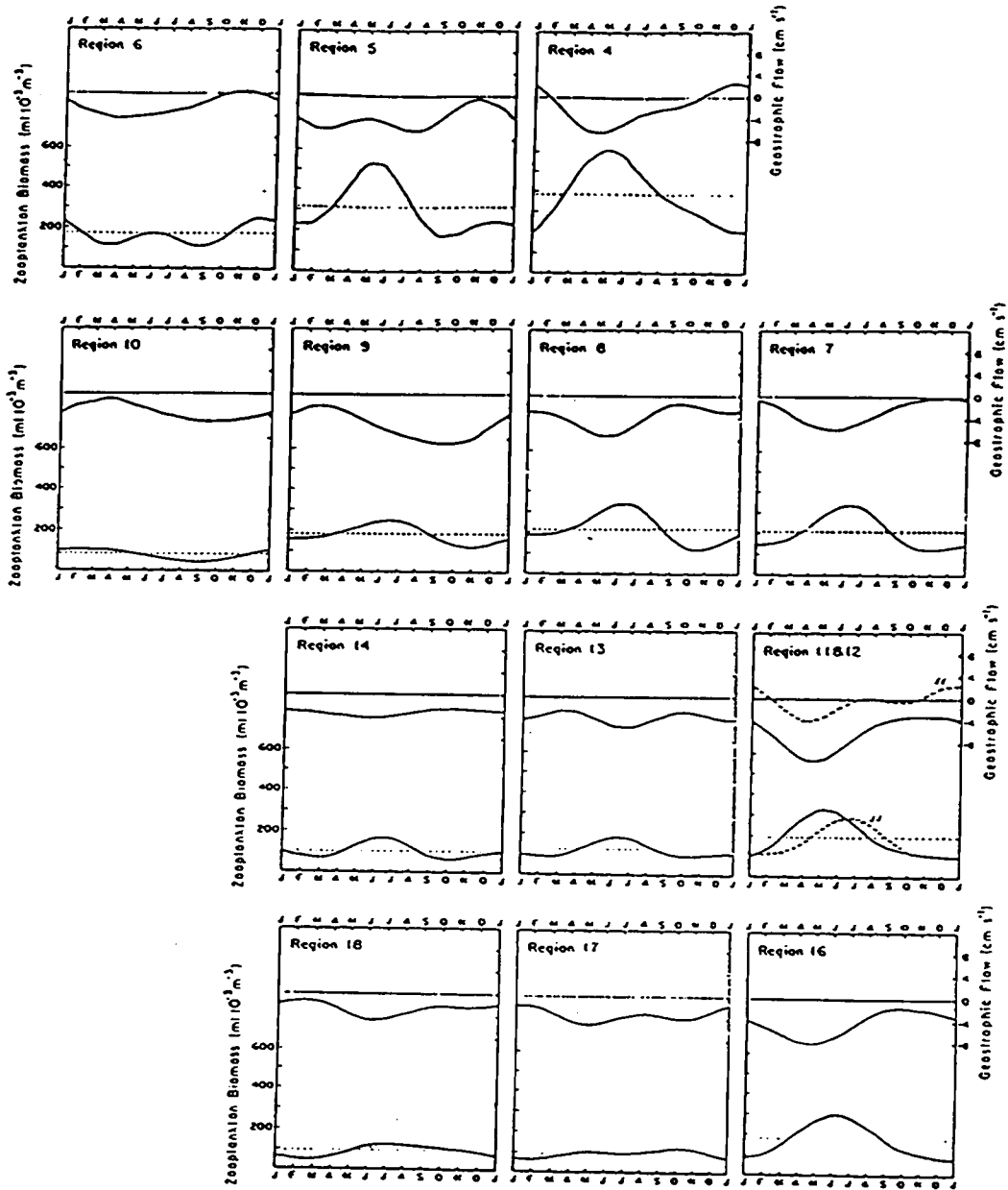


Figure 2 - Comparison of the seasonal cycles of zooplankton displacement volume and alongshore geostrophic flow in the 14 regions used by Roesler and Chelton (1987), their Figure 6.

series of geostrophic flow for passive advection to be the controlling mechanism.

This expected 90° phase shift can be qualitatively explained as follows. Suppose the alongshore velocity, v , varies as

$$v = \sin(\omega t + \theta)$$

where t is time, ω is the annual frequency and θ is the phase of the annual cycle. In the Data Description and Methods section, it is shown that the advection of zooplankton biomass, ζ , is related to the alongstream velocity by

$$\frac{\partial \zeta}{\partial t} = -\frac{\partial}{\partial y} \cdot (v\zeta) = -v \cdot \left(\frac{\partial \zeta}{\partial y} \right).$$

Assuming that the seasonal variations of $\frac{\partial \zeta}{\partial y}$, are small (i.e., $\frac{\partial \zeta}{\partial y}$ is approximately constant), then

$$\frac{\partial \zeta}{\partial t} \approx -\frac{\partial \zeta}{\partial y} \sin(\omega t + \theta).$$

Integrating with respect to t , it is apparent that ζ lags v by 90°. The similarity in the phase of the alongshore geostrophic flow and zooplankton biomass thus suggests that processes other than passive advection must be important to zooplankton variability. This is not necessarily the case, however, since this simple analysis neglects cross-shore transport, Ekman transport and time variations in $\bar{v}\zeta$.

Because of limitations in the CalCOFI sampling strategy, previous studies of large-scale zooplankton variability have neglected the effects of energetic mesoscale variability now known to exist in the California Current. Over the

past decade, a large amount of research in the California Current system has focused on the coastal transition zone between the warm surface waters of the open ocean and the cold freshly upwelled waters off the coast. Advanced Very High Resolution Radiometry (AVHRR) and Coastal Zone Color Scanner (CZCS) satellite imagery have revealed the existence of large cold water filaments extending hundreds of kilometers offshore along the west coast of the United States during the spring-summer upwelling season (Abbott and Zion, 1985, Traganza et al., 1983). Several studies have shown that intense, narrow seaward flowing jets are associated with the filament structure (Davis, 1985; Huyer, et al., 1991; Kosro et al. , 1991) as well as energetic eddies (Huyer, 1984; Kosro and Huyer, 1986). Extensive research conducted on these cold filament/jet structures has provided evidence that these features are a dominant and persistent component of eastern boundary current regions.

Studies by the Coastal Transition Zone Group (1988) off northern California, have indicated that the filament and jet structures off Point Arena, California, are an integral part of the generally continuous equatorward flowing jet at the core of the California Current. CZCS satellite images have shown that high concentrations of phytoplankton pigments off northern California occur in narrow jets of cold water and are bordered by strong fronts on one or both sides (Abbott and Zion, 1985). These findings suggest that the strong jet acts as a boundary between the more northern offshore, low phytoplankton and zooplankton biomass waters and the nearshore, recently upwelled, high phytoplankton and zooplankton biomass waters found to the south and inshore of the jet (Hood et al., 1990; Chavez et al., 1991; Mackas et al., 1991). Zooplankton biomass levels within the jet are as high as in the

nearshore region and extend along the jet axis. In addition, the surface characteristics of water within the jet are similar to water properties north of the region, suggesting a history of alongshore advection.

Smith and Lane (1991) suggested that filament frontal zones may act to focus secondary production by aggregating reproductive zooplankton adults. As noted above, high levels of phytoplankton and zooplankton biomass are consistently found within the jet during the period of strongest offshore flow. Smith and Lane also found that reproductively active copepod adults were transported from the nearshore region to approximately 370 kilometers offshore in July of 1988. Washburn (1991) estimated that 5-11 days are required for a 320 km displacement in the surface layer of the jet. Slightly longer displacement times of 12-21 days were noted for movement along constant density surfaces. These results suggest that if production is enhanced in the jet and it carries its populations well offshore, then these jets may contribute a large quantity of zooplankton biomass to the California Current and eastern North Pacific Ocean in a relatively short time.

Although the exact spatial and temporal seasonal occurrence of the filament/jet structures is not yet fully understood, the results from the Coastal Transition Zone studies have provided evidence that mesoscale events in flow patterns of the California Current, occurring over relatively short time scales, may have a dramatic influence in determining the seasonal variability of zooplankton biomass. The contribution of these offshore-displaced zooplankton populations to local production in the southward flowing California Current has yet to be determined. Still, a significant transport of reproductively active zooplankton populations from the nearshore to the

offshore region is likely to influence the observed zooplankton production of the California Current region.

It should be noted that the filament and jet structure studied by the Coastal Transition Zone Group lies to the north of the present study region. These northern jets may transport zooplankton to the northern California Current, where they could then be advected downstream into the study region. However, similar cold filament signatures have been observed in AVHRR and CZCS images in the CalCOFI study region (Pelaez and McGowan, 1986; Moum et al., 1988; Strub et al., 1990). Thus, filament and jets along the central California coast could contribute to seasonal zooplankton variability in the present study region in the same manner as has been observed off northern California.

Clearly, the dominant mechanisms controlling the observed seasonal zooplankton variability in the California Current have not been determined. Does passive advection or local production (via nutrient advection and primary production) of zooplankton play any significant role in determining the observed seasonal cycles in biomass, or is rapid offshore advection of zooplankton by narrow, intense jets more important? This study quantitatively examines the hypothesis that advection of zooplankton by the large-scale California Current is the controlling mechanism of the variability in the seasonal cycle of zooplankton. The method used is similar to the box model used by Roemmich (1989) in an investigation of mass, heat, salt, and nutrient flux off southern California using CalCOFI data from 1984-87. A close balance between seasonal variability in the observed zooplankton and variations in the seasonal advective transport of zooplankton would indicate

that passive advection is the dominant mechanism. An imbalance would indicate that local zooplankton production and/or injections from nearshore regions by jets is responsible for the seasonal variability. Note that this simple budget cannot provide any information about the details of the biological processes occurring within the box.

DATA DESCRIPTION AND METHODS

1. CalCOFI Data Description

Probably the most extensive simultaneous physical and biological long-term data set in the world has been acquired by the California Cooperative Oceanic Fisheries Investigations (CalCOFI). Since 1949, CalCOFI has been collecting vertical profiles of temperature, salinity and oxygen as well as total macrozooplankton net tows over the region extending from San Francisco to the tip of the Baja peninsula. The unique feature of the CalCOFI data set is its fixed sampling grid (Figure 3). Surveys are conducted along parallel lines separated by 74 km, extending approximately 500 km from the coast. Frequently sampled lines, 'cardinal' lines, are separated by approximately 222 km.

Unfortunately, the temporal sampling scheme has not remained constant over the past 42 years. The first ten years of sampling (1950-1960) were conducted at monthly intervals with few interruptions. From 1961 to 1969, the sampling strategy switched to 3 month intervals. Due to financial constraints, CalCOFI moved to monthly sampling every 3 years in 1969. The 3-year sampling scheme has continued to the present for the full CalCOFI region. In 1984, CalCOFI added quarterly surveys each year of lines 77 and 93 and an offshore line parallel to the coast connecting these two cross-shore lines to the sampling scheme. Sampling of nutrients, chlorophyll-a and primary productivity was initiated in 1981 and has been routinely maintained at all

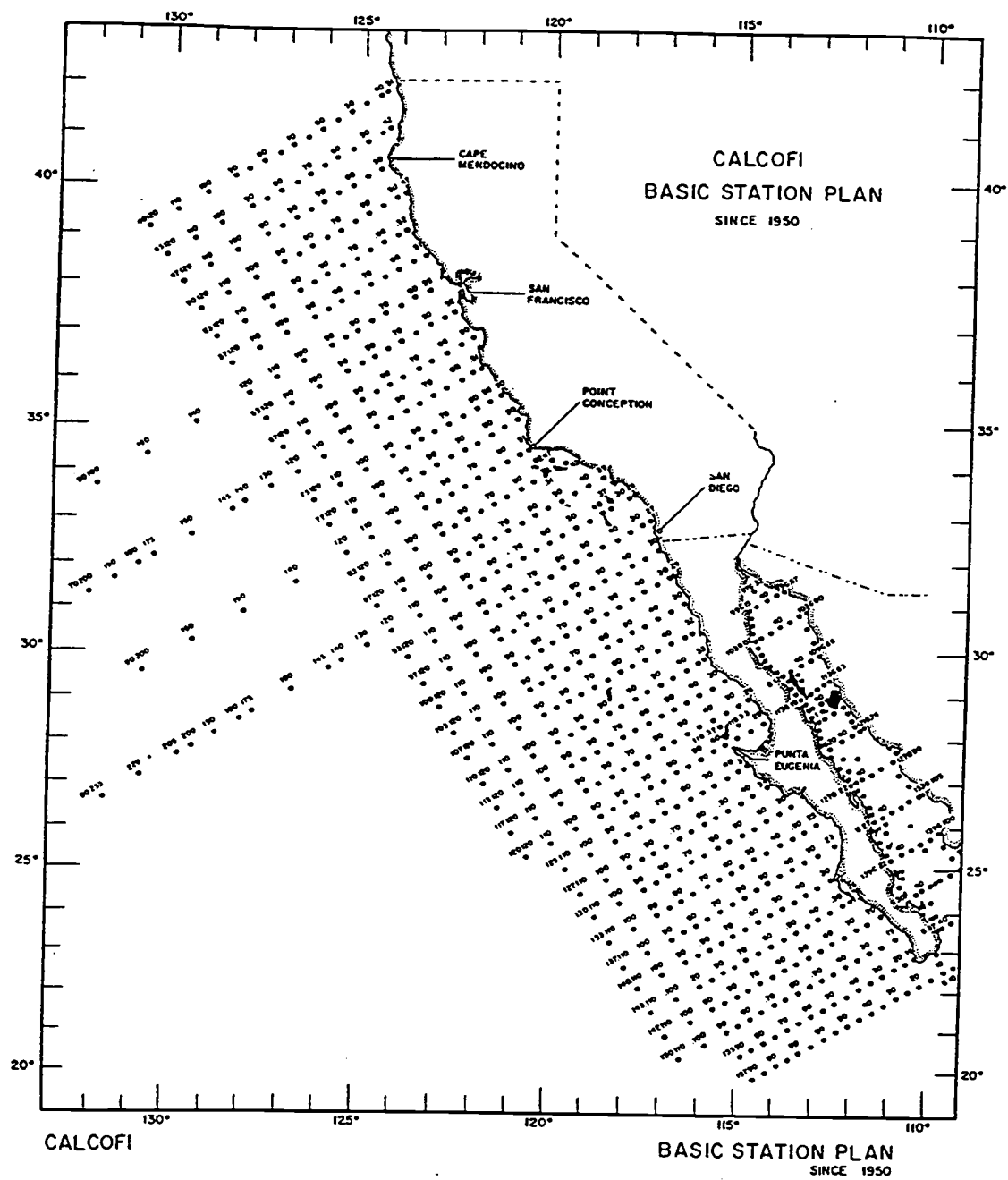


Figure 3 - CalCOFI geographic sampling grid indication line and station locations. Taken from CalCOFI Reports (1988).

hydrographic stations since 1984. This study utilizes CalCOFI data collected from 1950 to 1982.

Zooplankton displacement volumes are measured using oblique net tows from a depth of 140 m to the surface. The nets are made of 500- μm mesh and are 5-m long with a 1-m diameter opening. The nets are retrieved at 20 m per second with a ship tow speed of 2 knots, filtering a total volume of approximately 500 m^3 of water. Zooplankton displacement volumes used in this study consist of the total zooplankton biomass retrieved minus all zooplankton exceeding 5 cc and all adult and juvenile fish. These data were kindly provided by Paul E. Smith at the National Marine Fisheries Service in La Jolla, California in 23 spatial regions as monthly averages over the 32 year time series.

Not all the CalCOFI hydrographic stations were occupied during any given sample month. Stations occupied more than 34 times between 1950 and 1982 were used in this study (Figure 4). At each station, specific volume and density (the reciprocal of specific volume) were computed at each observed sample depth down to 500 m from the vertical profiles of temperature and salinity. The specific volume anomaly was calculated as the difference between the observed specific volume and the specific volume of a standard seawater sample with temperature of 0° C, and a salinity of 35 parts per thousand. The 32 year mean at each station as well as monthly seasonal values of specific volume anomaly were calculated at each sample depth.

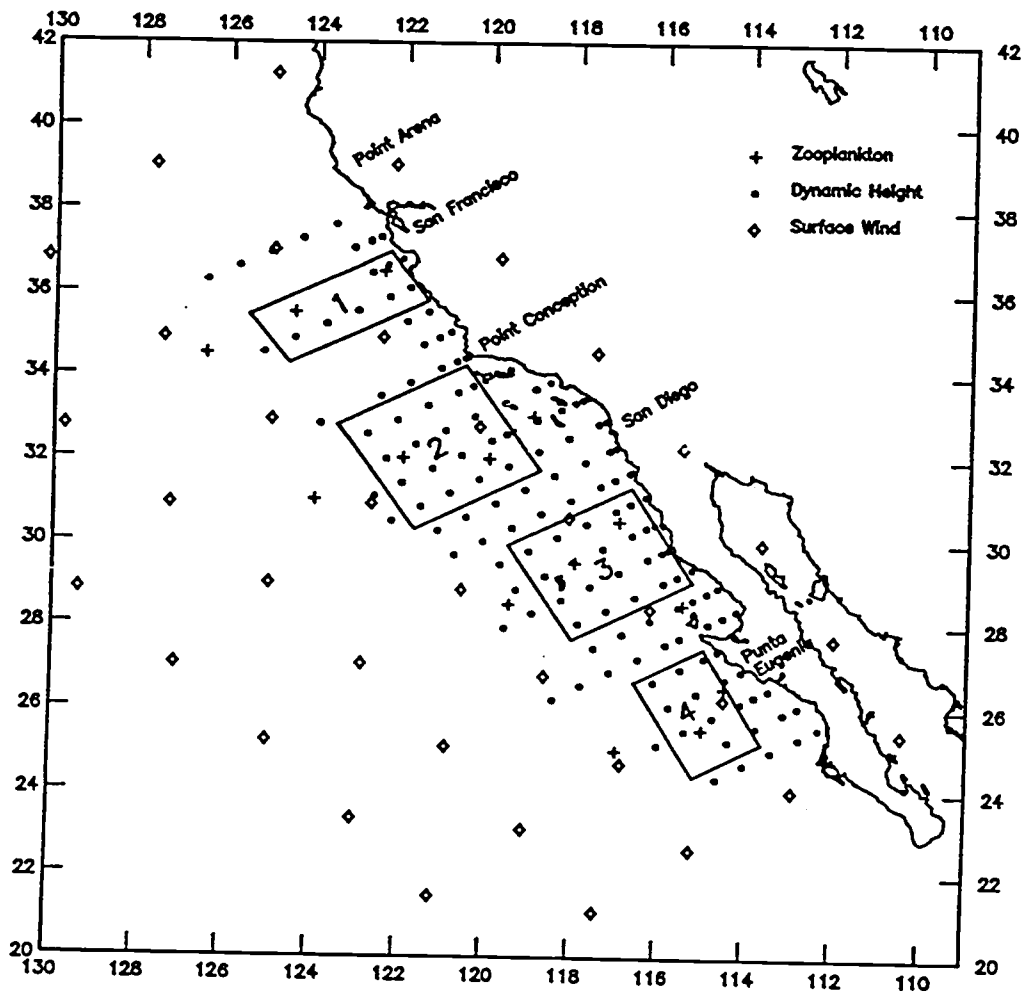


Figure 4 - CalCOFI zooplankton and dynamic height as well as FNOC marine surface winds data point locations used in this study. Also shown are the geographical locations of the four box model study areas labeled 1, 2, 3 and 4.

2. FNOC Wind Data Description

Fleet Numerical Oceanography Center (FNOC) marine surface layer winds were provided by Don Vanderpool at Goddard National Space Data Center in Greenbelt, Maryland. This data are on an approximately 380 km spaced grid (Figure 4) over the study region, covering the period from 1950 to the present. The time series of wind data was chosen to match the temporal sampling period of the CalCOFI zooplankton and hydrographic time series.

3. Region Descriptions

To examine the north-south flux of zooplankton in the California Current, four regions were chosen located near the coast (Figure 4). Each region was chosen to be a rectangular box with a fixed volume. Boxes are oriented 30 degrees from the normal coordinate plane so that the inshore and offshore faces are roughly parallel to the coast, while the north and south faces are approximately perpendicular to the coast. North in this sense denotes the more northern face of the box. The vertical extent of each region was chosen to be equal to the greatest depth of zooplankton sampling (140 m). The alongshore and cross-shore dimensions as well as the volume of each region are summarized in Table 1.

Table 1 - Horizontal dimensions and volume of each box model region.

	North/South length (km)	East/West length (km)	Volume (km)
Region 1	310	150	6.51E+03
Region 2	320	320	1.43E+04
Region 3	270	320	1.17E+04
Region 4	180	290	7.31E+03

4. Derivation of Box Model Equations

Consider a small rectangular box with volume V , fixed in space in a moving fluid with dimensions ∂x , ∂y and ∂z . The change in the concentration of a specific property, Q , is the difference between the sources and sinks of Q inside V and the flux of Q through V . Assuming the flow through V is incompressible, then the conservation of Q can be represented as:

$$\begin{aligned} \frac{\partial Q}{\partial t} &= \sum Q_{\text{sources}} - \sum Q_{\text{sinks}} - \bar{\nabla} \cdot (Q\bar{U}) \\ &= \sum Q_{\text{sources}} - \sum Q_{\text{sinks}} - \left[\frac{\partial(Qu)}{\partial x} + \frac{\partial(Qv)}{\partial y} + \frac{\partial(Qw)}{\partial z} \right] \end{aligned} \quad (1)$$

where t is time and u , v and w are the components of vector velocity \bar{U} parallel to the x , y and z coordinate axis.

Conservation of Mass

Changes in the mass of V can be caused by changes in the pressure and heat and by salt ion exchanges. These variations produce minor fluctuations in mass in comparison to the average density of the water (Pond and Pickard, 1989). For the purpose of this study, these small variations have been neglected and the mass of the ocean within in V is assumed to be constant. The time rate of change of mass within V is then zero, or is said to be in steady state (i.e. there are no sources or sinks of mass).

$$\frac{\partial \rho}{\partial t} = \sum \rho_{\text{sources}} - \sum \rho_{\text{sinks}} = 0$$

By substituting mass (ρ) for Q , in equation 1:

$$\bar{\nabla} \cdot (\bar{U}\rho) = \left[\frac{\partial(\rho u)}{\partial x} + \frac{\partial(\rho v)}{\partial y} + \frac{\partial(\rho w)}{\partial z} \right] = 0 \quad (2)$$

This is the equation of continuity which states that the total mass divergence through V must equal zero.

To calculate the continuity equation over a volume, an estimate of vertical velocity is necessary. The vertical velocity integrated over the area of each region is assumed to be zero. The reasoning behind this assumption is that the average vertical velocity in the ocean is much smaller than the average horizontal velocity. Generally, the ratio of depth to horizontal distance of the ocean is of the order 10^{-3} or less. This is because the scale of the vertical velocity is of the order of 10^{-3} or less of the horizontal velocities over the whole ocean. In any case, no measurements of vertical velocity were available from the CalCOFI data set. Possible errors associated with this assumption are discussed in detail in Appendix A.

To test whether mass is conserved in each model region, equation 2 must be integrated over the volume of each region.

$$\iiint_{zyx} \bar{\nabla} \cdot (\bar{U}\rho) \, dx dy dz = 0.$$

To simplify this calculation, the Divergence Theorem (also known as Gauss's Theorem) is invoked, which states that the divergence over a specified volume is equal to the area integral of the flux normal to each face (Kundu, 1990),

$$\iiint_{zyx} \bar{\nabla} \cdot (\bar{U}\rho) \, dx dy dz = \int_A (\bar{U}\rho) \cdot \hat{n} \, dA \quad (3)$$

where A is the surface area and \hat{n} is the normal vector to each face. Note that in the following derivations, the normal vector was chosen to be directed into the box on each face opposite the usual convention. This convention was

adopted so that a positive transport value would indicate an accumulation in the box, and a negative value would denote a loss.

As the top of each box lies at the ocean surface, mass flux through this face must equal to zero. Recalling that flux through the bottom is assumed to be zero, the integral on the right hand side of equation 3 becomes the sum of the integral of mass flux through the north (N), south (S), east (E) and west (W) faces.

$$\int_{A_N} (\bar{U}\rho) \cdot \hat{n} dA_N + \int_{A_S} (\bar{U}\rho) \cdot \hat{n} dA_S + \int_{A_E} (\bar{U}\rho) \cdot \hat{n} dA_E + \int_{A_W} (\bar{U}\rho) \cdot \hat{n} dA_W = 0 \quad (4)$$

where A_N , A_S , A_E , and A_W are the incremental areas on the N, S, E, and W faces of the box.

This equation was used to calculate geostrophic mass balance in each of the box model regions. An explanation of how geostrophic velocities were calculated from the CalCOFI data is given in the Computational Details section below. To simplify the calculation of equation 4, a constant vertical profile of horizontal velocity over 0-140 m equal to the surface geostrophic velocity value was assumed to be a reasonable first-order estimate. As the geostrophic velocity is not dependent on depth in this simplified model, the area integrals in equation 4 can be represented as the product of the line integral and depth ($h=140$ m) of the north, S_N , south, S_S , east, S_E , and west, S_W , sides of each box. The model for geostrophic mass divergence used in this study then reduces to:

$$h \int_{S_N} \bar{v}_g \rho dS_N + h \int_{S_S} \bar{v}_g \rho dS_S + h \int_{S_E} \bar{u}_g \rho dS_E + h \int_{S_W} \bar{u}_g \rho dS_W = 0 \quad (5)$$

where h is the depth of the box, and \bar{v}_g and \bar{u}_g are the surface geostrophic velocity vector components perpendicular to the north/south and east/west faces respectively. Geostrophic mass balance on a daily time step was obtained in each of the box model regions using the calculation shown in equation 5 within computer round off error.

Conservation of Zooplankton Volume

Substituting zooplankton concentration, ζ , in equation 1, the variation in zooplankton over time can be represented as:

$$\begin{aligned} \frac{\partial \zeta}{\partial t} &= \sum \zeta_{\text{sources}} - \sum \zeta_{\text{sinks}} - \bar{\nabla} \cdot (\bar{\mathbf{U}} \zeta) \\ &= \sum \zeta_{\text{sources}} - \sum \zeta_{\text{sinks}} - \left[\frac{\partial(\zeta u)}{\partial x} + \frac{\partial(\zeta v)}{\partial y} + \frac{\partial(\zeta w)}{\partial z} \right] \end{aligned} \quad (6)$$

Short-term (< a month) variations in zooplankton concentration in the ocean are often large in the horizontal and vertical scales, with fluctuations often an order of magnitude greater than the seasonal mean. Therefore, a steady state balance of zooplankton cannot be assumed. As with the conservation of mass calculation, the top and bottom boundaries of each box are closed to flux ($w=0$) in the simple model used here. Integrating both sides of equation 6 over volume:

$$\iiint_{z y x} \frac{\partial \zeta}{\partial t} dx dy dz = \iiint_{z y x} (\sum \zeta_{\text{sources}} - \sum \zeta_{\text{sinks}}) dx dy dz - \iiint_{z y x} \bar{\nabla} \cdot (\bar{\mathbf{U}} \zeta) dx dy dz$$

As noted above, estimates of zooplankton displacement volume were obtained by CalCOFI using continuous net tows from 140 m to the surface. Bulk zooplankton measurements obtained from a net tow do not provide information about the vertical distribution of zooplankton. As a first order estimate,

zooplankton are assumed here to be uniformly distributed over 0-140 m, with integrated concentrations equal to the net tow measurement. This assumption is discussed in more detail in Appendix A.

The working hypothesis of this study is that variability in seasonal zooplankton volume is due entirely to advection of zooplankton. In this model, no sources or sinks of zooplankton are present, in which case

$$\iiint_{zyx} \frac{\partial \zeta}{\partial t} dx dy dz = - \iiint_{zyx} \bar{\nabla} \cdot (\bar{U} \zeta) dx dy dz$$

To the extent that the appropriate scales of \bar{U} and ζ are resolved by the CalCOFI data, any imbalance in the above equation implies the existence of sources or sinks of zooplankton biomass within the volume, possibly from unresolved mesoscale variability.

Following the conservation of mass derivation, the right hand side of this equation can be written using the Divergence Theorem as the surface area integral over the four vertical faces of each box.

$$\iiint_{zyx} \frac{\partial \zeta}{\partial t} dx dy dz = - \int_A \bar{U} \zeta \cdot \hat{n} dA$$

In the surface layer of the ocean, zooplankton are subject to horizontal transport due to geostrophic and Ekman transport. The velocity term in each of the area integrals on the right-hand side of this equation can therefore be divided into geostrophic and Ekman transport components. As noted above, a constant vertical profile of geostrophic velocity (equal to the surface velocity) was chosen. Transport of zooplankton due to Ekman forcing is confined to the layer of frictional influence of the wind, called the Ekman layer. The depth of

the Ekman layer, or the effective depth of the wind-driven current, depends on the eddy viscosity and the latitude. At middle latitudes, the depth of the Ekman layer may occur at depths greater than 140 meters during strong wind events (Pond and Pickard, 1983). As a first-order estimate, the depth of the Ekman layer is assumed here to be less than 140 meters. Thus, Ekman transport of zooplankton is assumed to be confined to within the greatest vertical extent of each region, 140 meters.

With these assumptions, the model for the time rate of change in observed zooplankton in each region becomes:

$$\begin{aligned} h \int_A \frac{\partial \zeta}{\partial t} dA &= - \int_A \bar{U} \zeta \cdot \hat{n} dA \\ &= - \left[h \int_S (\bar{v}_g \zeta) \cdot \hat{n} dS + \int_S (\bar{T}_{\text{Ekman}} \zeta) \cdot \hat{n} dS \right] \end{aligned} \quad (7)$$

where \bar{v}_g is surface geostrophic velocity normal to each face (directed out), h is depth (140 m), and \bar{T}_{Ekman} is the wind driven Ekman vertically-averaged velocity normal to each face (S). As in the calculation of geostrophic mass transport, a positive transport equates flux into the box, and negative denotes flux out on all four of the vertical faces. In order to allow for comparisons between different regions, both sides of equation 7 were normalized by the volume of each box to obtain the time rate of change of total zooplankton displacement volume within the box.

5. Computational Details

Zooplankton (ζ)

Zooplankton net tow measurements were averaged into 23 spatial regions for each CalCOFI sampling month over the 32 year time series. Roesler and Chelton (1987) determined that 14 of the 23 spatial zooplankton volume averages had sufficient data to resolve the seasonal cycle. Following the method of Roesler and Chelton, the full 32-year time series of zooplankton was used in each region to estimate the seasonal cycle by least squares regression on an annual and semiannual cycle plus a constant offset (mean zooplankton volume). It should be noted that these seasonal cycles contain only four degrees of freedom. Due to the limited degrees of freedom, statistical comparisons between two seasonal cycles cannot be analyzed to infer cause-and-effect relationships with any degree of reliability. This is discussed in detail in Chelton (1982). It is nonetheless useful to analyze the CalCOFI hydrographic and zooplankton data to examine the validity of the hypothesized advective model for zooplankton variability.

Zooplankton regression coefficients for the seasonal cycles were first interpolated from the 14 gridded raw zooplankton areas to a 75 km grid over the study region using cubic spline interpolation. The data were smoothed to minimize the influence of small-scale features introduced by noise in the estimate of regression coefficients. Regression coefficients on the 75 km grid were then interpolated to a fine-mesh 10 km grid using Laplacian interpolation and were smoothed again. This double interpolation and smoothing procedure was subjectively found to be the most reliable method of

reproducing reasonable contours of the zooplankton seasonal cycle on the high-resolution 10 km grid used here to investigate the validity of equation (7). A discussion of the reliability of this interpolation scheme can be found in Appendix B.

The time rate of change of zooplankton volume within each box region (left-hand side of equation 7) was calculated on a daily time step. In each box region, zooplankton change was calculated as simple first differences between the area integral of zooplankton displacement volume (times 140 m) computed for two consecutive days from the interpolated seasonal cycle regression coefficients. The last day of the year was differenced with January 1. The units of zooplankton displacement volume and the change in zooplankton displacement volume used throughout this study are thus ml/1000 L and ml/1000 L/day respectively.

Geostrophic Velocity (\bar{u}_g , \bar{v}_g)

Integration of specific volume anomaly over 0-500 db pressure range results in values of dynamic height at the sea surface relative to the 500 db level. The seasonal cycle regression coefficients of 0/500 db dynamic height were obtained following the method used for zooplankton. The regression coefficients were interpolated to a 10 km grid using cubic spline interpolation. Each of the dynamic height coefficient fields were heavily smoothed after interpolation to minimize the presence of any small scale features. Increasing the resolution of the dynamic height data causes velocity estimates to be more sensitive to observational errors in temperature, salinity and pressure and sampling errors arising from energetic transient mesoscale variability. Such

errors introduce noise in the estimated regression coefficients. This noise should be minimized by the large amount of smoothing applied here.

Horizontal gradients in dynamic height are proportional to the magnitudes of geostrophic flow at the sea surface relative to flow at 500 db (assumed to be small). Geostrophic flow was computed from dynamic height gradients using:

$$\bar{u}_g = -\frac{g}{f} \frac{\partial h}{\partial y}$$

$$\bar{v}_g = \frac{g}{f} \frac{\partial h}{\partial x}$$

where \bar{u}_g and \bar{v}_g are the cross-shore and alongshore geostrophic surface velocities, $\frac{\partial h}{\partial y}$ and $\frac{\partial h}{\partial x}$ are horizontal gradients of dynamic height, f is the Coriolis parameter ($2\Omega \sin(\text{latitude})$, where Ω is the Earth rotation rate), and g is gravitational acceleration. The large latitudinal extent of the study region precluded the use of a constant Coriolis parameter for all four study regions due to the β effect. The latitude in the calculation of the Coriolis parameter was chosen to be the center latitude of each region.

As the 500 db pressure level is roughly equal to the pressure at 500 m, geostrophic velocity calculations can only be computed between two stations in water deeper than 500 m. Over the continental shelf and upper continental slope, many of the CalCOFI stations have a bottom depth less than 500 m. Rather than extrapolating the offshore dynamic heights onto the shelf, this study limits geostrophic velocity calculations to stations in water deeper than 500 m.

Calculating geostrophic velocity by differencing two dynamic height grid points results in a velocity value centered between the two data points. This produces a spatial shifting of the two velocity vector grids of half the grid spacing (5 km) for each gridded velocity component. The u velocity grid is shifted in the y direction and the v grid is shifted in the x direction. Since the present model requires that zooplankton and velocity (normal to each face) data be on the same grid, the zooplankton values at the two dynamic height data points used to compute geostrophic velocity, were averaged to obtain values of zooplankton and velocity at the same centered grid point. Units of geostrophic velocity are m/day.

Ekman Transport (\bar{T}_{Ekman}^x , \bar{T}_{Ekman}^y)

A total of 36 FNOC marine surface layer wind grid points were used to calculate wind stress over the study region. By assuming a neutral stability of the air, sea surface wind stresses in the east/west and north/south directions were calculated from vector winds at each of the 36 grid points using:

$$\tau^x = C_d \rho_a |\bar{U}| u$$

$$\tau^y = C_d \rho_a |\bar{U}| v$$

where C_d is the drag coefficient as defined by Large and Pond (1981), ρ_a is density of the air above the sea surface (assumed a constant of 1.223 kg / m^3), and u and v are the east and north components of the vector wind velocity \bar{U} . The 32-year time series of wind stress at each FNOC grid point was used to form the seasonal cycle by the same least squares regression model as zooplankton and dynamic height.

Ekman transport is defined as surface wind stress divided by the product of the Coriolis parameter times density of water, and is directed 90° to the right of the wind stress in the northern hemisphere. Assuming that Ekman transport is confined to the Ekman layer (assumed to be less than 140 m), the integrated east and north Ekman transport, calculated in m²/day, can be defined as:

$$\bar{T}_{\text{Ekman}}^x = \frac{\tau^y}{f\rho_w}$$

$$\bar{T}_{\text{Ekman}}^y = -\frac{\tau^x}{f\rho_w}$$

where ρ_w is the density of the water (assumed a constant of 1025 kg/m³) and f is the Coriolis parameter calculated as in the geostrophic velocity computation. Seasonal regression coefficients of wind stress were used to compute Ekman transport coefficients at each FNOC grid point. These coefficients were then gridded by Laplacian interpolation to the 10 km zooplankton and dynamic height grid. As seasonal cycles of wind stress and Ekman transport are quite smooth and well behaved, no smoothing of the interpolated FNOC data was necessary.

6. *Estimating Local Zooplankton Growth/Loss*

The observed zooplankton biomass time series within each box was calculated by spatially integrating zooplankton over the volume of each box. The estimated zooplankton displacement volume in each region from advection can be obtained by time integration of the right-hand side of equation 7. The

difference between the observed and advected zooplankton biomass time series is a measurement of local growth or loss of zooplankton within each box,

$$\zeta_{\text{local}}(t) = \zeta_{\text{obs}}(t) - \zeta_{\text{adv}}(t). \quad (8)$$

Local sources of zooplankton in this context denote any general growth processes, such as weight increase of individuals and abundance increase, that result in increased volume. Local sinks of zooplankton include a wide range of biological processes that are very difficult to quantify. A few of the more important processes include natural death, predation, and vertical migration. The actual source or sink processes cannot be identified or quantified from the bulk zooplankton biomass estimates obtained in the CalCOFI surveys. Therefore, a local source connotes bulk accumulation or growth in zooplankton, while a sink represents a general loss of zooplankton.

Recall that the time series of observed zooplankton and transport (geostrophic and Ekman) are formed by a regression on an annual and semiannual seasonal cycle plus a constant offset. This constant offset term in both time series represents the yearly mean, and thus is independent of time in the seasonal case. Multiplication of these two time series results in time independent coefficients. These coefficients become linearly dependent on time in the time integral of advective zooplankton transport. The existence of linearly dependent time coefficients would imply that zooplankton biomass due to advection in each region increases or decreases linearly with time (depending on the signs of the constant terms). This apparent paradox is a consequence of the fact that the net advection of zooplankton does not average to zero over the seasonal cycle. In turn, this implies that some biological

process must be occurring inside each box that balances this linear component of advection in the steady state mean. While the biology implied by the existence of these linear terms is of great interest, this is not part of the seasonal variability that is the primary focus of this study. Moreover, the CalCOFI data set lacks the information necessary to investigate these biological processes in detail. Therefore, the linear terms were removed in the calculation of zooplankton due to advection. For a detailed mathematical derivation of these linear terms and their biological implications, see Appendix C.

The unknown constant of integration in the estimate of advected zooplankton also presents a problem. The mean of the advected zooplankton must be equal to the mean of the observed zooplankton if the hypothesized advection of zooplankton is valid. The constant of integration was therefore evaluated on this basis, thus yielding the best possible comparison between observed and advected zooplankton biomass.

RESULTS

The results are divided into five sub-sections. In section 1, the large-scale seasonal patterns of zooplankton displacement volume, dynamic height, geostrophic velocity, wind stress and Ekman transport over the study area are described. Section 2 compares the time series of geostrophic and Ekman transport of zooplankton within each of the four model regions. In section 3, the net advective transport of zooplankton obtained from the model is compared with the observed time rate of change of zooplankton from the CalCOFI data. A comparison of the time rate of change of zooplankton and the net advection in each region and the phase of the observed and advected zooplankton seasonal cycles are given in section 4. The difference between the computed advective flux of zooplankton and the observed rate of change of zooplankton is an indication of zooplankton productivity from local biological processes occurring within each region. The seasonal cycles of zooplankton biomass due to advective and biological processes computed by integrating the time rates of change are described in section 5.

The limitations of the spatial and temporal scales of variability that can be resolved by this box model analysis should be emphasized. As the horizontal dimensions of the four regions range from 150 to 330 km, and are separated by an average of 170 km, the model can resolve only large scale patterns of variability. Furthermore, due to the limitations imposed by the grid spacing of the CalCOFI zooplankton data, only very large-scale patterns of the seasonal distribution of zooplankton can be resolved. Raw zooplankton displacement

volume data may resolve only the seasonal cycle at best, due to the limitations imposed by the sampling scheme and the pooling of zooplankton samples.

1. Large-scale seasonal patterns

The seasonal distribution of zooplankton displacement volume obtained from this study is the same as that found by Roesler and Chelton (Figure 5). A strong north-south gradient is present throughout the year with the highest zooplankton volumes consistently observed in the northern portion of the study area. Overlaid on this north-south gradient is a strong cross-shore gradient with the highest concentrations of zooplankton observed near the coast. The cross-shore gradient is strongest in spring and weakest in winter. Seasonal variations in zooplankton volume are greatest in the northern ($\sim 36^\circ$) and offshore regions.

Figure 6 shows the seasonal mean 0/500 db dynamic height contours with arrows indicating the direction of geostrophic flow. The seasonal trend of geostrophic flow found in this study is the same as the pattern described in other studies of the CalCOFI region (Hickey, 1979; Roesler and Chelton, 1987; Lynn and Simpson, 1987). The characteristic north to south flow of the California Current is observed throughout the year. This southward flow intensifies through spring to a maximum in summer, and slowly relaxes through fall. Southward flow is fairly broad from San Francisco to Point Conception. Nearshore poleward flow reversal occurs during the fall and winter months. A large shoreward component of flow occurs south of 33° N.

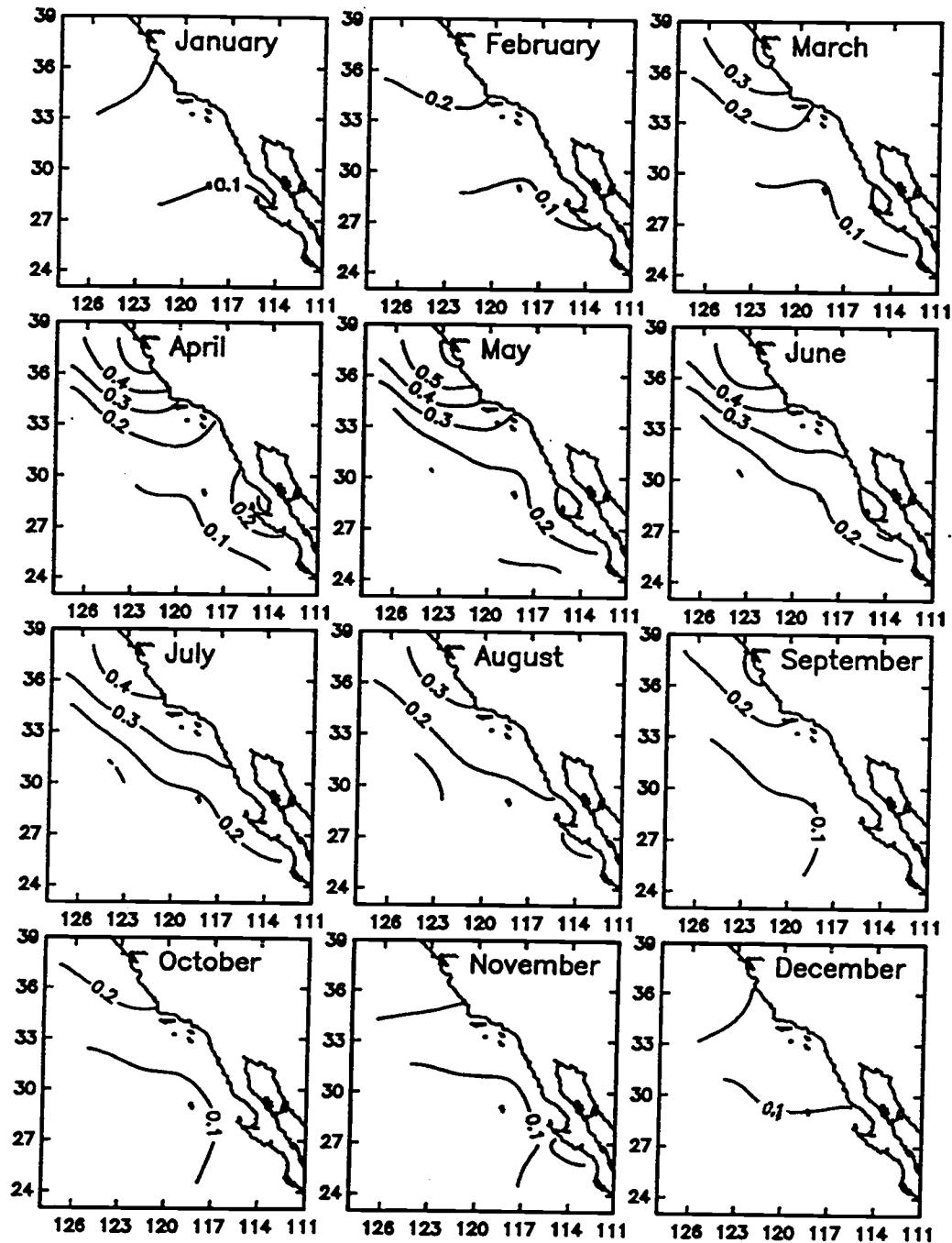


Figure 5 - Contour maps of zooplankton displacement volume using the 32 year record of the 14 areal averaged zooplankton data points regressed to an annual and semiannual seasonal cycle (plus a constant offset) interpolated to a fine mesh grid. Contour interval is 0.1 ml/1000 L.

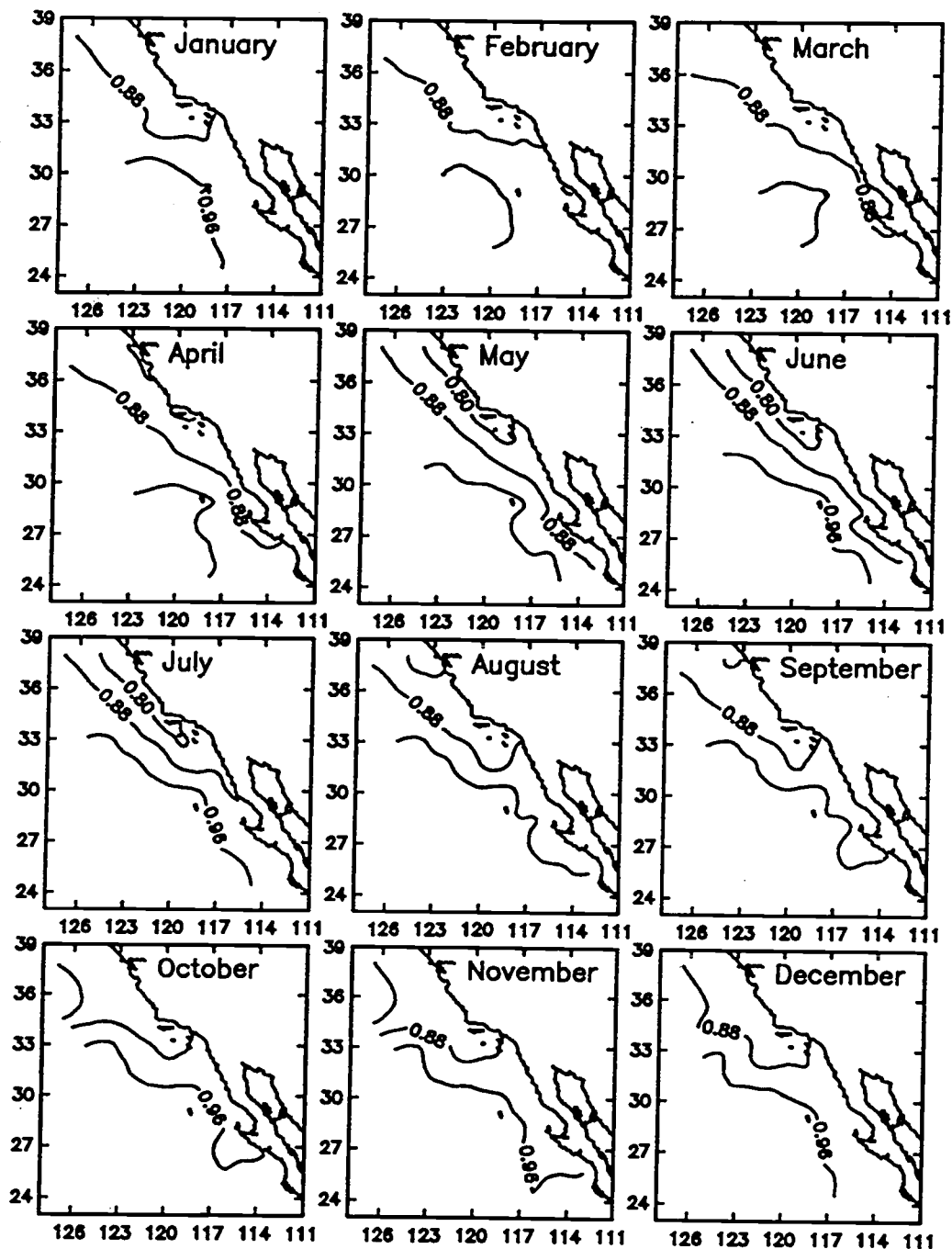


Figure 6 - Contour maps of 0/500 db dynamic height using the full 32 year record of the 149 dynamic height data points regressed to an annual and semiannual seasonal cycle (plus a constant offset) interpolated to a fine mesh grid. Contour interval is 0.08 m.

During summer, part of this flow turns northward in what appears to be the near-shore limb of the Southern California Eddy. The rest of the flow continues to move southward, intensifying as it nears the coast ($\sim 30^\circ$ N), and then meanders west as it encounters Punta Eugenia.

Wind stress is generally directed alongshore over most of the study region (Figure 7). Southeastward wind stress begins to increase in February, although the rate of increase is not uniform over the CalCOFI region. South of Punta Eugenia ($\sim 28^\circ$ N), wind stress is strongest in April, and weakest in August. Between Punta Eugenia and San Francisco, wind stress is maximum in May and June and minimum in winter. Wind stress magnitudes and directions are relatively uniform over the study region during fall and winter. A cross-shore gradient in wind stress is apparent during the spring and summer. Wind stress is most intense over the center of the strongest equatorward geostrophic flow, while near the coast and farther offshore the wind stress is consistently lower. As a consequence, the wind stress curl is positive near the coast and negative farther offshore.

Seasonal fields of Ekman transport indicate the general pattern of local wind-forced coastal upwelling. Mean transport is directed offshore over the CalCOFI region, indicating conditions are favorable for upwelling (Figure 8). During winter, offshore transport increases in strength from north of Point Conception to the Baja Peninsula with maximum values observed offshore of Punta Eugenia. The highest offshore transports are observed during spring with the region of maximum offshore transport located north of Point Conception. During summer, the region of maximum Ekman transport remains north of Point Conception, however the magnitude of these transports

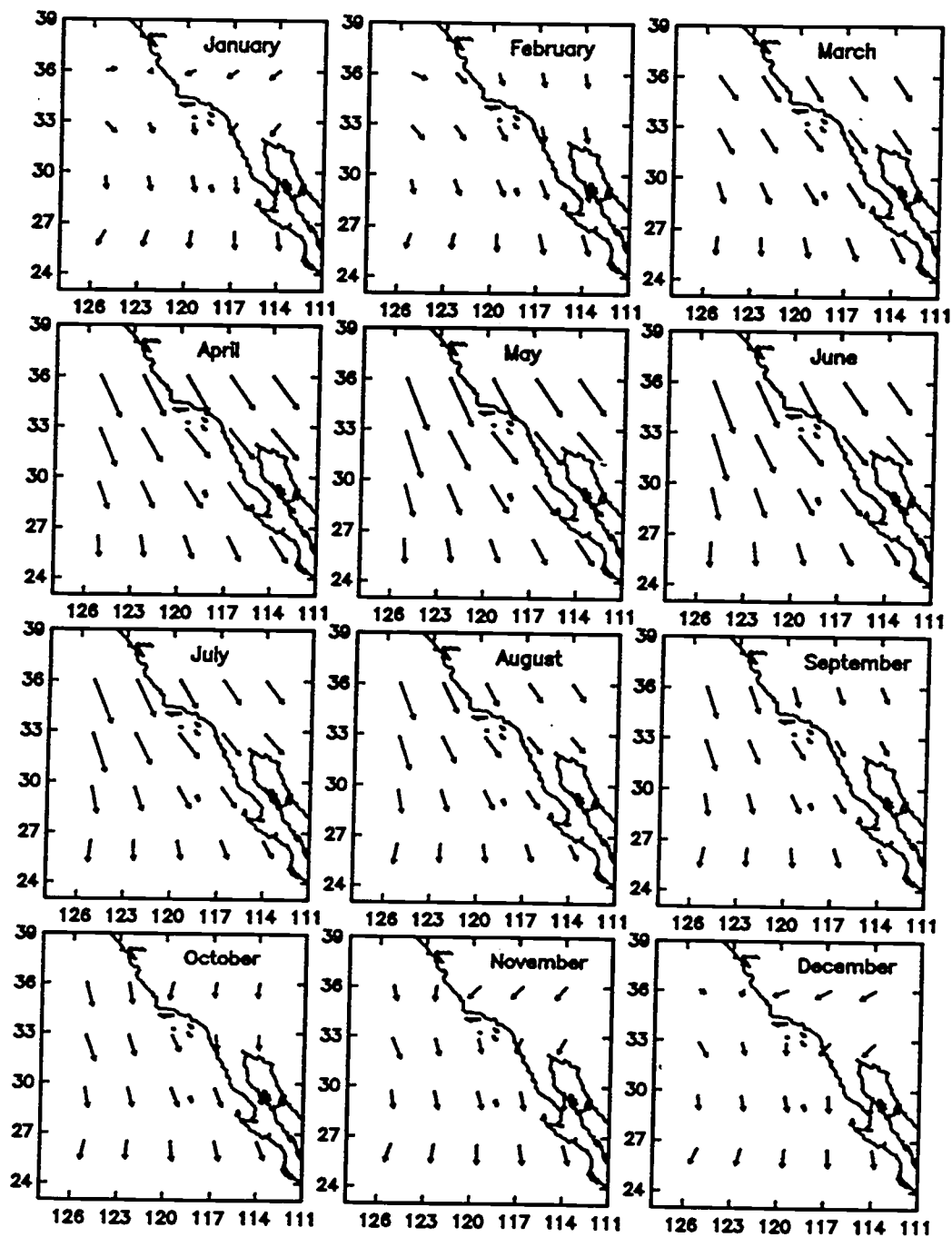


Figure 7 - Seasonal pattern of wind stress obtained from harmonic regressions of the 36 FNOZ marine surface data points and interpolated to a fine mesh grid. 1 inch = 0.4 N/m².

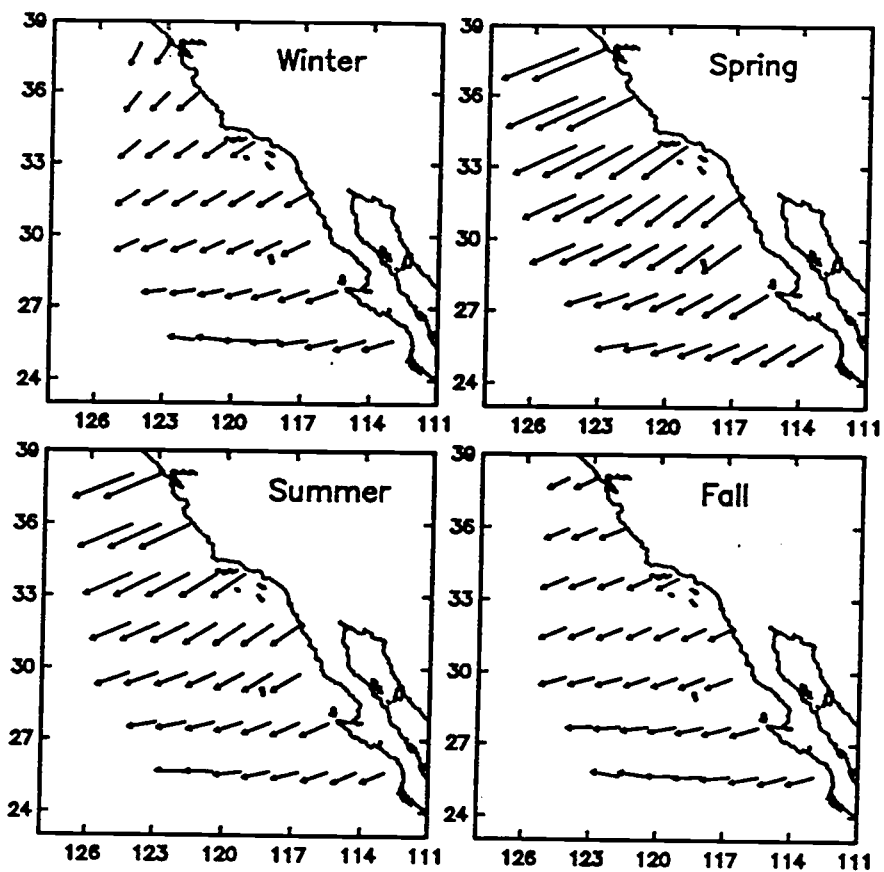


Figure 8 - Ekman transport averaged by season. Obtained using the interpolated wind stress values on the fine mesh grid. 1 inch = 4 m^2 /day.

has diminished considerably from spring. Offshore transport relaxes during the fall over the entire study region.

2. Geostrophic versus Ekman Zooplankton Transport

The hypothesis tested in this study is that the observed seasonal changes in zooplankton displacement volume are due to the advective transport of zooplankton. As this study focuses on the changes in zooplankton biomass in the upper surface layers of the ocean, both geostrophic and Ekman transport mechanisms are included in the advection calculation. In this section, a comparison between the net geostrophic and Ekman transport of zooplankton in each of the four study regions is presented to resolve the effect of each component on the observed seasonal change in zooplankton biomass.

Time series of net Ekman and geostrophic zooplankton transport for each region are shown in Figure 9. Negative values denote net transport of zooplankton out of the region (i.e. divergence of zooplankton transport), while positive values indicate net zooplankton transport into the region (i.e. convergence). Recall that the "north" and "south" faces are not perpendicular to geodesic normal coordinates. Rather, they run approximately perpendicular to the coastline; north in this sense denotes the more northern face of the box. The east and west faces are roughly parallel to the coast. Net geostrophic and Ekman zooplankton transports are normalized by the volume of each region to obtain the contribution of each to the time rate of change of zooplankton displacement volume.

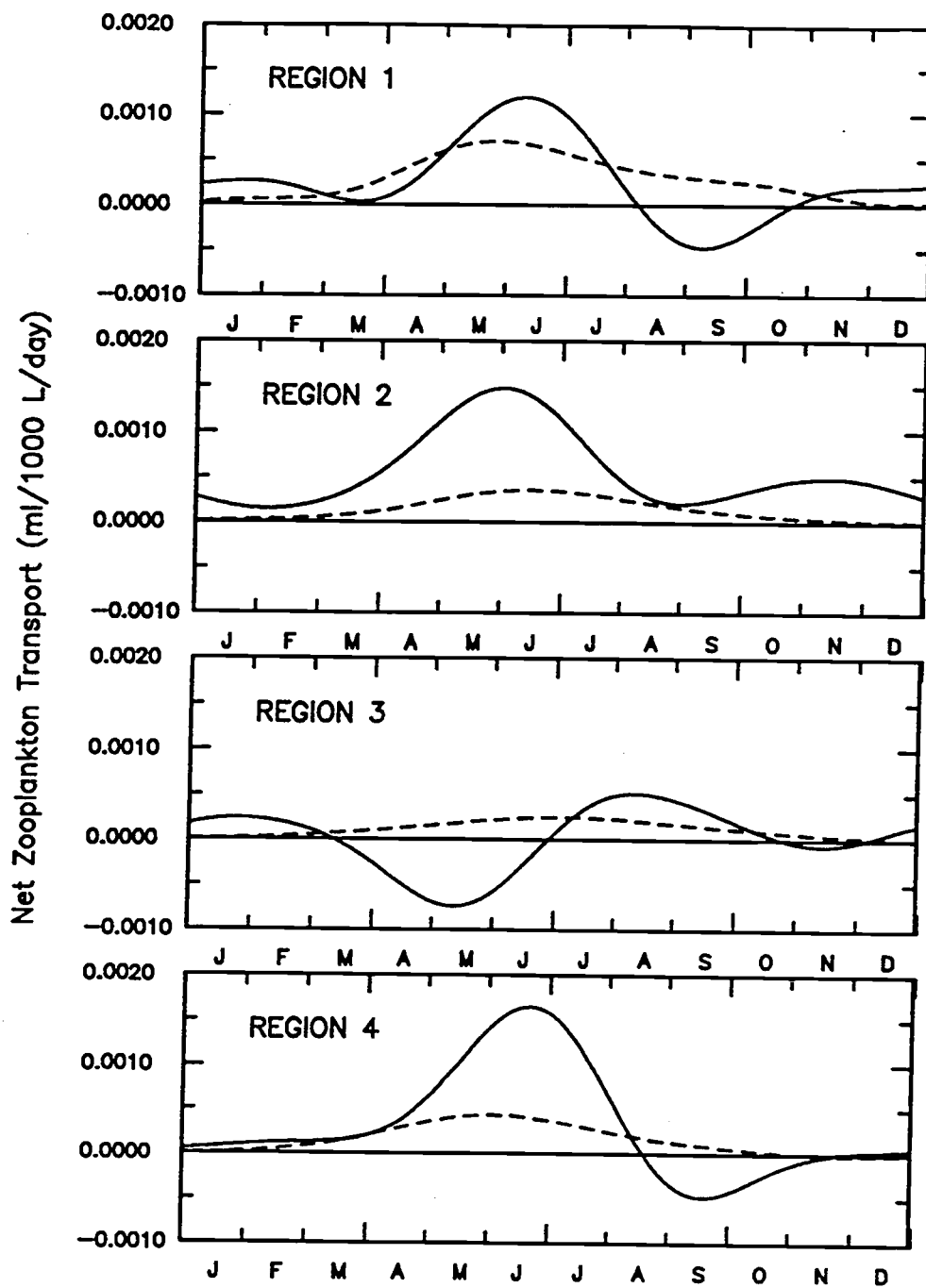


Figure 9 - Time series of net geostrophic (solid lines) and net Ekman (dashed lines) zooplankton transport obtained in each of the four model regions.

All four regions show a similar trend in net Ekman transport of zooplankton. Net Ekman zooplankton fluxes are consistently positive (i.e. convergence of zooplankton) with relatively small seasonal variations. Generally, net Ekman transport of zooplankton is high during spring and summer and low during fall and winter. The greatest net Ekman transport is observed in region 1, while the smallest is in region 3. As described above, wind stress is generally directed southward and increases offshore to a maximum approximately coincident in location with the strongest geostrophic flow. West of the cross-shore intensification, wind stress and Ekman transport gradually decline. A cross-shore gradient in zooplankton volume also exists with the highest volumes observed near the coast. Consequently, Ekman zooplankton transport out of the western face of each region is smaller than the gain through the eastern face. Thus, the net Ekman zooplankton transport increases the concentration of zooplankton in each region throughout the year.

Seasonal variations in net geostrophic zooplankton transport are much more dramatic. During winter, transport is low and fairly constant due to the low zooplankton abundance and relatively small horizontal velocities. From spring through fall, the net geostrophic transport in regions 1, 2 and 4 increases during spring to a maximum import in late spring to early summer. The largest transport observed in region 4. Net transport decreases sharply through summer to a minimum in fall.

The seasonal cycle of net geostrophic zooplankton transport in region 3 is quite different from that for the other three regions. Export is most intense during spring and is followed by a period of import during summer through

fall. Maximum export occurs approximately 1 month before the maximum import observed in the other regions. Conversely, the maximum import occurs roughly 1 month before the maximum export observed in other regions. The cause of this pattern is discussed in the following section (3).

3. Net Advection and Observed Zooplankton Productivity

The total zooplankton transport (geostrophic plus Ekman) through each region is referred to here as the net advective transport of zooplankton (NATZ). The results of the model (i.e. net advection of zooplankton) and the observed time rate of change of zooplankton calculated from the CalCOFI data are presented in this section. The advective transport of zooplankton through each face of a region is dependent on the concentration of zooplankton and the strength of advection perpendicular face. In an effort to elucidate the influence that these two factors have upon the NATZ, the alongshore and cross-shore gradients of zooplankton are presented, as well as the advective transport of zooplankton through each face. The change in the distributions of zooplankton within each region can be resolved in the time series of the alongshore and cross-shore zooplankton gradients. A positive value in the alongshore zooplankton gradient indicates higher biomass on the north as compared to the south. In the cross-shore zooplankton gradient, a positive value indicates higher zooplankton concentrations on the east face decreasing offshore.

A comparison of the time series of advective transport of zooplankton through each face indicates the alongshore and cross-shore patterns of zooplankton divergence. In the figures of advective zooplankton transport, negative values indicate transport out of the region (i.e. loss of zooplankton). Positive transport values denote transport into the region (i.e. accumulation of zooplankton). Zooplankton transport through each side has been multiplied by the surface area of each face and has units of ml m/1000 l/day. The time series of alongshore and cross-shore divergence and NATZ were normalized by the volume of each model region in order to obtain the change in observed zooplankton biomass by advection in units of ml/1000 l/day.

Region 1

The average concentration of zooplankton along the north face is consistently greater than along the south face in region 1, as indicated by the positive alongshore gradient in zooplankton (Figure 10a). The maximum alongshore gradient of zooplankton occurs in spring. A strong cross-shore gradient in zooplankton biomass also occurs in spring with a maximum roughly two times as large as the maximum alongshore zooplankton gradient. The sharp increase in the cross-shore gradient observed during late winter to early spring indicates that concentrations of zooplankton on the east face increase more rapidly than on the west face.

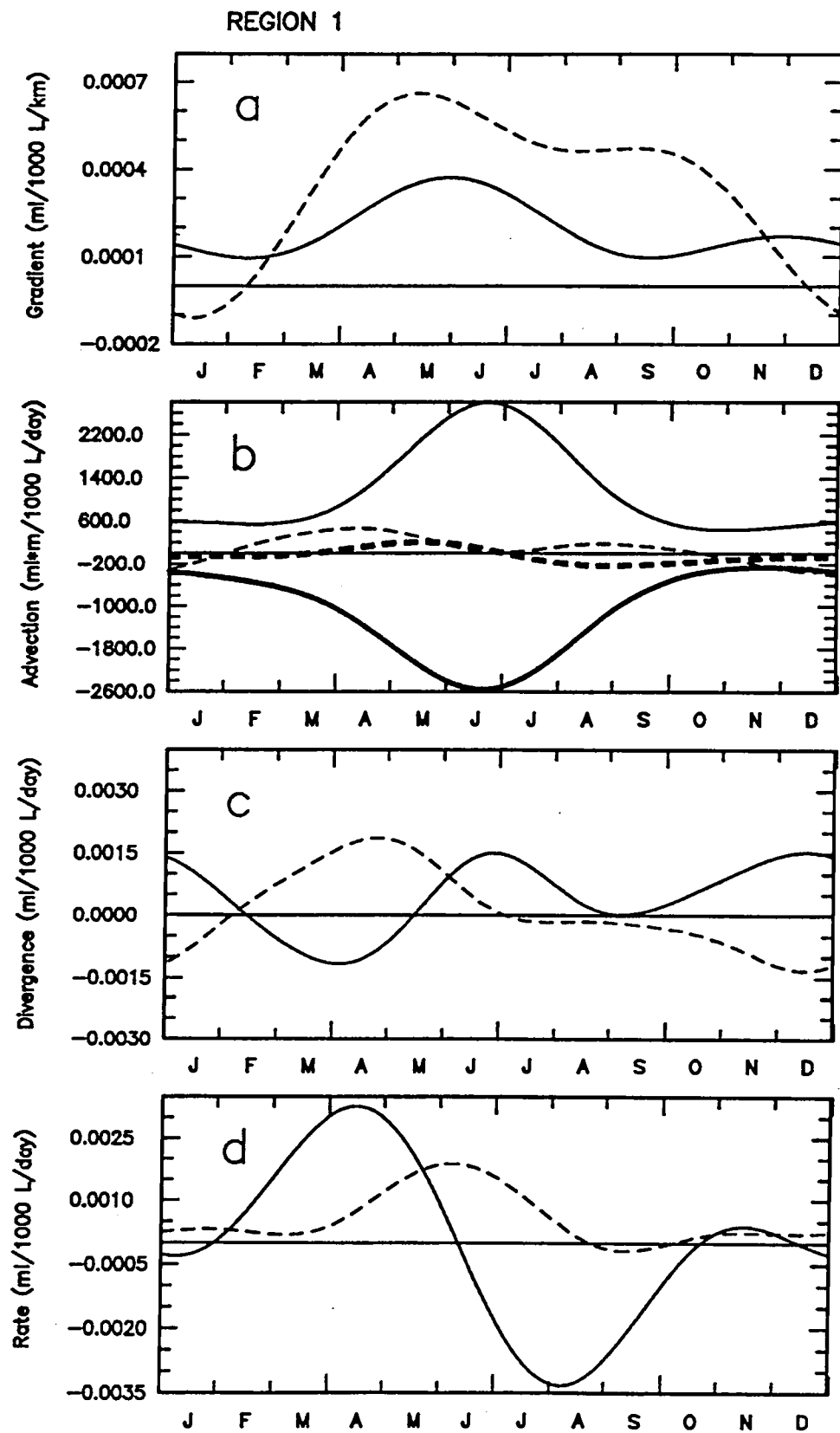
Advective transport of zooplankton in region 1 (Figure 10b) is dominated by a gain through the north and a loss through the southern face. Seasonal trends of transport across the north and south faces are roughly in phase and similar in magnitude. During winter, the alongshore transport is

Figure 10 - For region 1, *a*, the time series of alongshore gradient in observed zooplankton biomass, shown as a solid line, calculated as the difference between the north and south face average zooplankton concentration. The time series cross-shore gradient in observed zooplankton biomass, shown as a dashed line, is calculated as the difference of the east and west face average zooplankton concentrations.

b, time series of advective transport of zooplankton through the surface area of the north (solid line), south (thick solid line), west (dashed line) and east (thick dashed line) faces of region 1. Positive values indicate transport into the region, while negative values indicate transport of zooplankton out of the region.

c, time series of alongshore divergence in zooplankton biomass transport, shown as a solid line, calculated as the sum of the north and south face advective transport of zooplankton. The cross-shore divergence of zooplankton, calculated as the sum of the east and west face transports, is shown as a dashed line. Note that these time series have been normalized by the volume of region 1.

d, time series of the observed change in zooplankton biomass over the volume of region 1 (solid line) and the time series of the net advection of zooplankton through region 1 (dashed line).



fairly constant and low. Alongshore zooplankton transport increases during spring to a maximum in June, and gradually declines through summer. Cross-shore zooplankton transport is consistently less than the alongshore. Accumulation of zooplankton through the west face is observed in spring through fall, while the east face acts as a loss for the region from summer through winter and a slight supply in spring.

During spring, the loss of zooplankton through the south face is larger than the gain through the north, resulting in alongshore divergence of zooplankton (Figure 10c). Cross-shore convergence occurs in spring to early summer due to gain of zooplankton on both the west and east faces. Convergence in the NATZ increases during spring due to greater cross-shore convergence than alongshore divergence (Figure 10d). In late spring through summer, the supply of zooplankton through the north face is greater than the loss through the south, while the transport through the east face (loss) is roughly equal in magnitude to the gain on the west. Thus, a net convergence is observed in the NATZ in late spring through late summer, with the maximum occurring in early summer. In fall and winter, the NATZ is small due to a relative balance between the alongshore and cross-shore transport of zooplankton

The hypothesis of the model tested in this study is that the observed changes in zooplankton are due solely to the advection of zooplankton populations. If this hypothesis were correct, then the time series of observed rates of change in zooplankton displacement volume from the CalCOFI data should be comparable in phase and magnitude to the NATZ computed from the model. From Figure 10d, it is clear that the two time series are not in phase in

region 1. Instead, the two time series appear to be 90° out of phase with the NATZ lagging the observed change in zooplankton. The observed maximum rate of increase of zooplankton occurs in early spring, almost 2 months before the maximum in net advective supply of zooplankton. Note that the maximum in the time rate of change in the observed zooplankton is almost twice as large as the time-lagged maximum in the NATZ.

Region 2

The phase and amplitude of the alongshore gradient of zooplankton in region 2 (see Figure 11a) is very similar in amplitude and phase to that observed in region 1. The cross-shore gradient of zooplankton is rather different, increasing in spring to a maximum in early summer, and then gradually declining through fall. Note that the maximum in the cross-shore gradient in region 2 is smaller by almost a factor of two than the maximum observed in region 1.

As in region 1, the dominant advective gain of zooplankton is through the north face in region 2 (Figure 11b), although the magnitude is diminished by roughly 20%. The south face acts as a loss of zooplankton throughout the seasonal cycle and is consistently less than the gain through the north. Therefore, the alongshore transport of zooplankton is convergent over the seasonal cycle with a maximum occurring at the end of spring (Figure 11c). The cross-shore transport acts to supply zooplankton through the west face and remove zooplankton through the east face throughout most of the year. The magnitude of the loss of zooplankton through the east face is larger than the gain through the west. Consequently, the cross-shore transport is

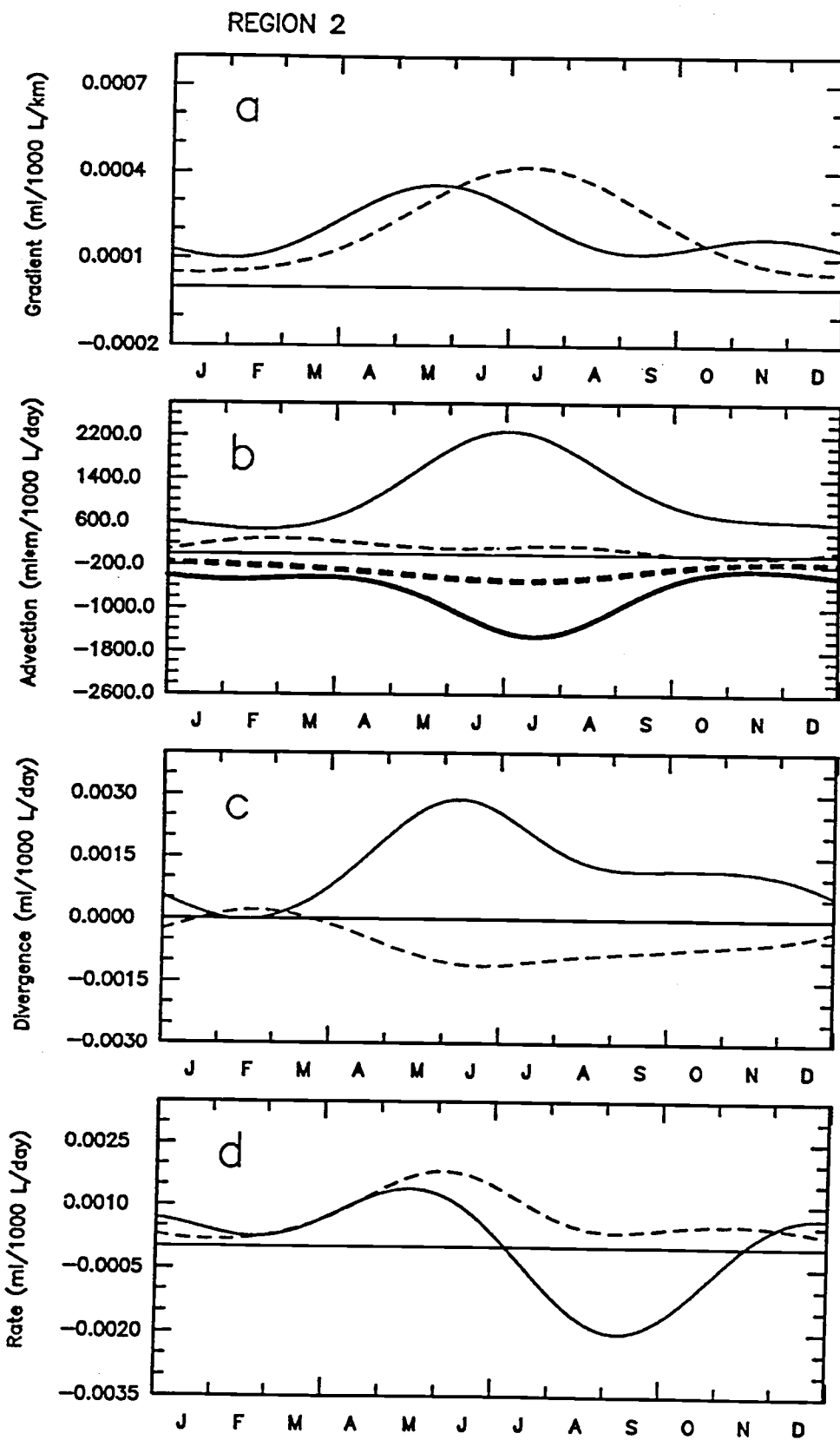


Figure 11 - Same as Figure 10, for region 2.

divergent in zooplankton throughout the year (Figure 11c). As the alongshore convergence of zooplankton is consistently greater than the cross-shore divergence, the resulting NATZ is consistently convergent with a maximum occurring in late spring (Figure 11d). Note that the peak in the NATZ is similar in phase and magnitude to the peak in region 1.

The observed time rates of change of zooplankton and NATZ are comparable in phase, but have different amplitudes (Figure 11d). The time rate of change of zooplankton displacement volume is maximal during late spring and minimal in August-September. A second smaller maximum is observed during winter. The NATZ is positive (supply of zooplankton) throughout the year, with the greatest transports observed in spring and summer. A close balance between the two time series is noted in early spring. The maximum NATZ is slightly greater than the maximum observed rate of change and is lagged by a few weeks.

Region 3

The time series of the alongshore zooplankton gradient observed in region 3 is dramatically different from the corresponding time series for regions 1 and 2 (Figure 12a). The negative alongshore gradient values observed during the spring indicate that the concentrations of zooplankton on the south face are greater than the concentrations on the north face. The positive values of the alongshore zooplankton gradient during winter and summer through fall indicate that higher concentrations of zooplankton are observed on the north face as compared to the south face. Note that the magnitude of the fluctuations in the alongshore gradient of zooplankton is

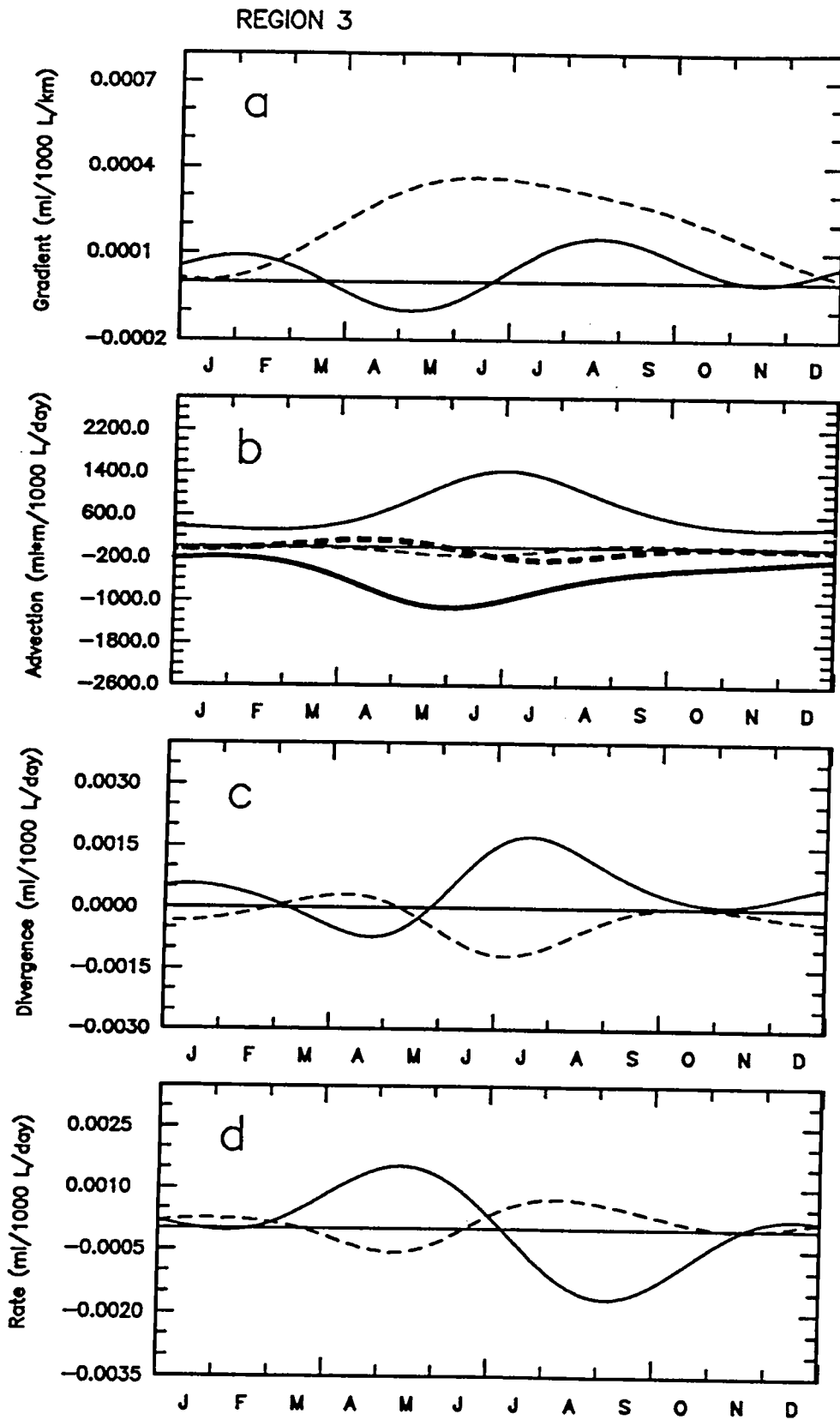


Figure 12 - Same as Figure 10, for region 3.

similar to those observed in regions 1 and 2. However, the annual average value in region 3 is smaller than the annual average observed in regions 1 and 2 and the alongshore gradient of zooplankton changes sign seasonally in region 3.

The cross-shore gradient in zooplankton is more similar to that of regions 1 and 2 than is the alongshore gradient. The cross-shore gradient intensifies in spring, with higher concentrations of zooplankton occurring on the east face. A maximum in the cross-shore gradient occurs in late spring/early summer and gradually declines to zero in mid winter indicating a uniform cross-shore concentration of zooplankton.

Transport of zooplankton through the north face is similar in phase with regions 1 and 2, with the magnitude of the peak in zooplankton supply slightly reduced from region 2 (Figure 12b). The pattern of loss through the south face leads the corresponding time series observed in regions 1 and 2 by approximately one month. As a result, the greatest loss through the south occurs about a month before the maximum transport through the north face. Therefore, as observed in region 1, the alongshore transport of zooplankton is divergent in spring and convergent in summer. The seasonal trend of transport through the east face is similar to region 1, but is shifted one month later. A loss in zooplankton generally occurs through the west face throughout the year.

As in region 1, the alongshore and cross-shore patterns of zooplankton divergence are approximately opposite in phase (Figure 12c). The amplitude of alongshore divergence is consistently greater than cross-shore divergence.

This amplitude offset is large enough to cause a rather surprising trend in the NATZ (Figure 12d). During spring, the peak in the cross-shore convergence occurs slightly before the peak in the alongshore divergence and is lesser in magnitude. This produces a divergence in the NATZ in region 3. In summer the pattern reverses, whereby the alongshore convergence is greater than the cross-shore divergence, resulting in a convergent flux of zooplankton.

The observed rate of change in zooplankton and the NATZ are nearly 180° out of phase in region 3 (Figure 12d). The maximum observed rate of increase of zooplankton biomass occurs in spring. During this period, the model shows a net decrease in zooplankton biomass due to advective processes. The opposite trend is observed in summer and fall. Rates from the model and CalCOFI observations are also out of phase in winter, although the amplitudes of each are much lower.

Region 4

The time series of the alongshore and cross-shore gradients of zooplankton observed in region 4 are very similar in phase, with the cross-shore gradient lagging the alongshore gradient by less than a month (Figure 13a). The strongest alongshore and cross-shore zooplankton gradients occur in late spring/early summer, with the amplitude of the cross-shore gradient larger than the alongshore gradient. Note that the maximum alongshore gradient occurs about one month later than the maximum in region 2, while the maximum cross-shore gradient in region 4 occurs one month earlier than in region 2. The magnitude of the cross-shore gradient in zooplankton observed in region 4 is also greater than the maximum observed in region 2.

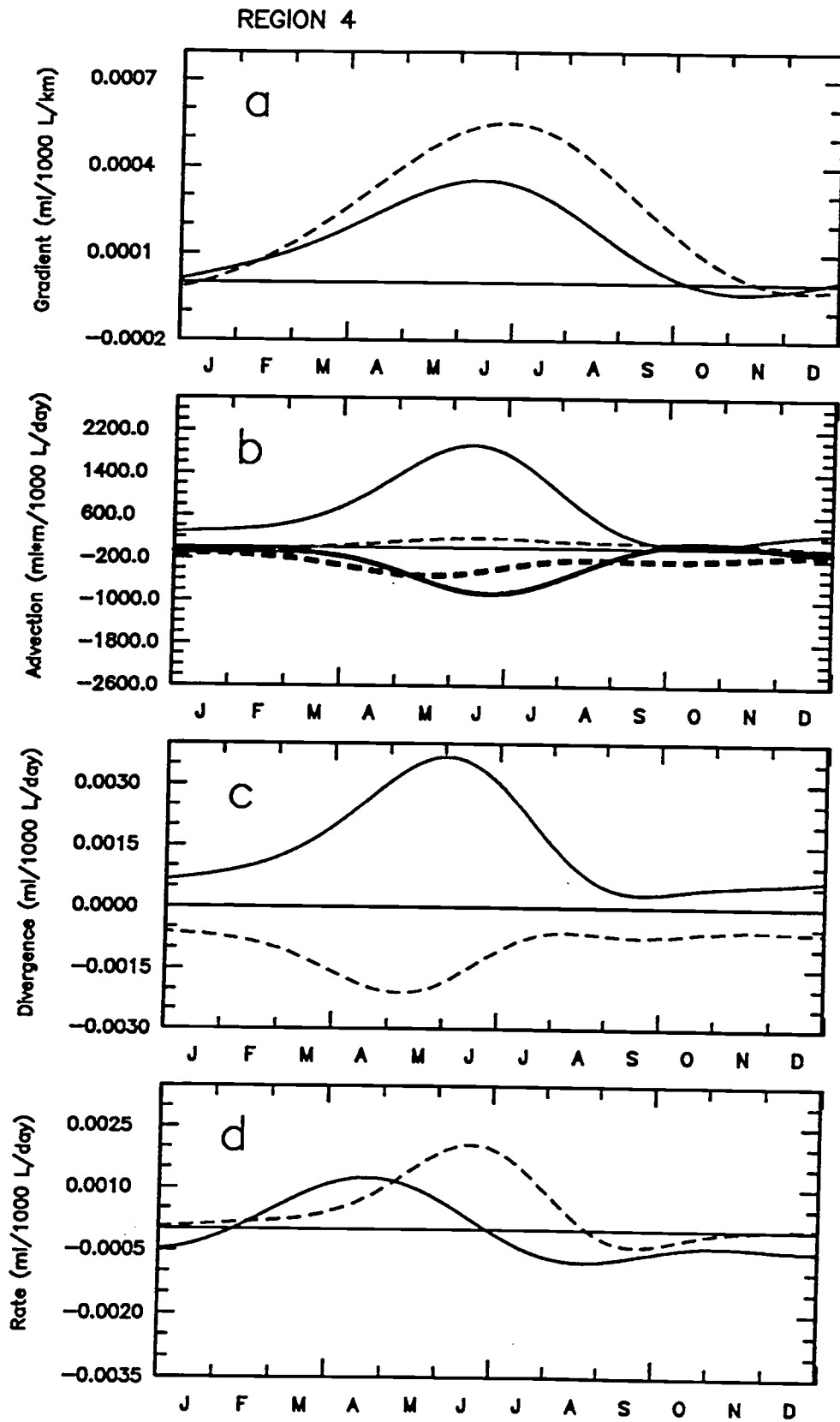


Figure 13 - Same as Figure 10, for region 4.

The peak in the dominant north face transport in region 4 occurs slightly earlier than the maxima observed in the other three regions (Figure 13b). In general, transport through the south face acts to remove zooplankton from the region. The amplitudes of zooplankton loss through the south and east faces are similar. However, the maximum in export through the south is less than one half the corresponding import on the north. As in region 2, the east face consistently shows advective loss of zooplankton. The maximum export through the east face leads the maximum observed on the south face by approximately one month. A consistently low supply of zooplankton is transported through the west face.

The seasonal trend of alongshore convergence of zooplankton observed in region 2 is also observed in region 4. However, the magnitude is consistently greater (Figure 13c). During winter, the amplitudes of alongshore convergence and cross-shore divergence are roughly equal, and thus the NATZ is negligible (Figure 13d). In spring, an increase in zooplankton biomass due to alongshore convergence is more rapid than the reduction in biomass due to cross-shore divergence, producing an increase in NATZ. The slight offset in the phase and magnitude of the alongshore transport and cross-shore transports cause a convergent maximum in the NATZ to occur during late spring.

The observed rate of change in zooplankton in region 4 is positive (i.e. an increase in zooplankton) only in late winter and spring (Figure 13d). The negative maximum rate of change of observed zooplankton biomass occurs in summer and is roughly half of the positive maximum. As in region 1, the maximum in the NATZ occurs 2-3 months after the maximum in the time rate of

change in zooplankton. However, unlike region 1, the magnitude of the maximum advective supply is greater than the rate of change of zooplankton biomass.

4. Zooplankton Productivity via Local Biological Processes

From the comparisons between the computed advective flux of zooplankton and the observed time rate of change of zooplankton in the previous section, large-scale advection of zooplankton clearly cannot fully explain the variability in the observed seasonal cycle of zooplankton in the four regions studied. The hypothesis of the model is that changes in zooplankton biomass in each region are due only to large-scale advection. Local sources/sinks of zooplankton have been neglected within each model region. Since the phase and amplitude of the change in observed zooplankton and the NATZ time series do not coincide in any of the four regions over the entire seasonal cycle, local sources/sinks of zooplankton must be a factor in determining seasonal variations in the observed zooplankton populations. The difference between the observed rate of change in zooplankton and the NATZ should provide an estimate of the rate of zooplankton gain/loss from local biological processes occurring within each region.

The differences between the observed zooplankton time rate of change and the NATZ in each region are shown in Figure 14. A positive difference indicates a local source (i.e. growth), while a negative difference indicates a local sink (e.g. predation, natural death) of zooplankton.

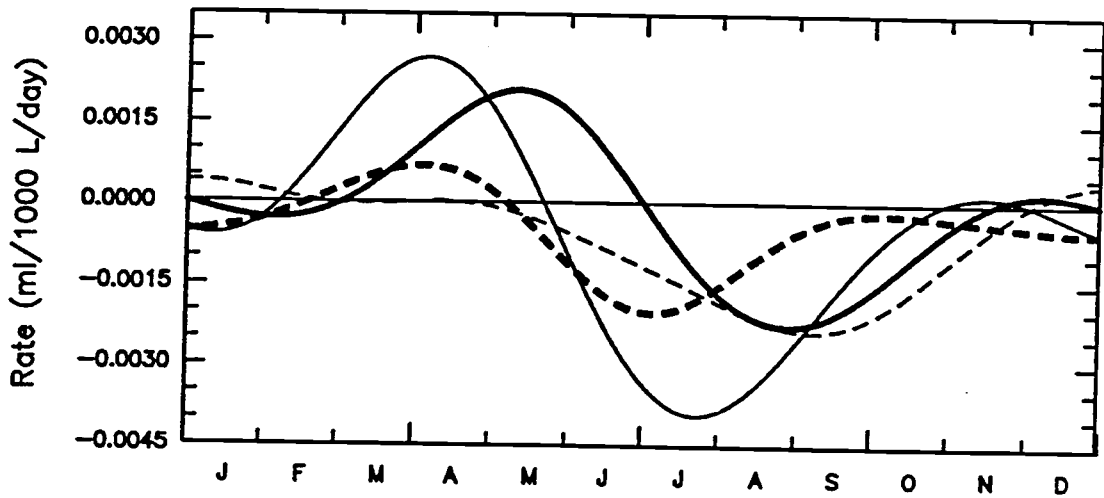


Figure 14 - The difference between the change in the observed zooplankton biomass and the net advection of zooplankton time series, shown in Figures 10-13, panel d, for each of the four model study regions. The difference time series for region 1 is drawn as a solid line, region 2 as a dashed line, region 3 as a thick solid line and region 4 as a thick dashed line.

The general pattern of local growth of zooplankton in the California Current, as determined from the residual calculation described above, can be summarized as follows. All four regions show negative local growth rates during the late summer to fall period. Regions 1, 3 and 4 show positive local growth rates during the spring to early summer period. There is no period of significant positive local growth in region 2.

The regional local growth rates can be summarized in detail as follows. In region 1 (Figure 14; solid line), large local growth is observed from late winter through mid spring. A maximum growth rate of approximately 0.003 ml zooplankton/1000 L/day is observed in mid spring. From late spring through early fall, the difference time series is negative, indicating local loss of zooplankton. In region 2 (dashed line), a close balance between the observed change in zooplankton and the NATZ occurs in early spring. In mid spring, the rate of zooplankton loss begins to increase reaching a maximum of about 0.0025 ml/1000 L/day at the beginning of fall. In region 3 (thick line), local zooplankton growth is observed during the spring, reaching a maximum rate in May of 0.002 ml/1000 L/day. This is followed by a period of loss until the end of fall. A period of local supply is observed in region 4 in late winter and early spring but the maximum in the rate of supply never exceeds 0.001 ml/1000 L/day (thick dashed line).

5. Zooplankton Seasonal Cycles

From Figures 10-13, it is evident that the annual mean advective transport of zooplankton is greater than zero in each region. A positive mean in the advective transport implies a linear increase in zooplankton concentration when integrated over the seasonal cycle. As discussed previously in section 6 of Data Description and Methods, this secular increase must be balanced by a loss at the same rate from biological processes within each region (i.e. mortality and predation). This secular term is not a part of the seasonal cycle and is thus neglected in the seasonal cycle of zooplankton biomass computed here from the advective flux of zooplankton biomass.

The seasonal cycle of zooplankton obtained by time integration of the advective flux of zooplankton is very similar in all four regions (Figures 15a, 16a, 17a, and 18a). The model produces a predominantly one cycle per year fluctuation in advected zooplankton in each of these regions. Minima in the advected zooplankton occur in early spring, while maxima are found in early summer.

A strong alongshore gradient in the observed zooplankton is present during spring and summer in regions 1, 2 and 4 with the highest concentrations occurring in region 1. The maxima in the local component occur in late spring in these regions, slightly before the corresponding maxima in the observed zooplankton (Figures 15b, 16b and 18b). The minimum in the local component of zooplankton occurs in mid fall in regions 1 and 2. The largest variations in the seasonal trend of local zooplankton concentrations occur in region 1.

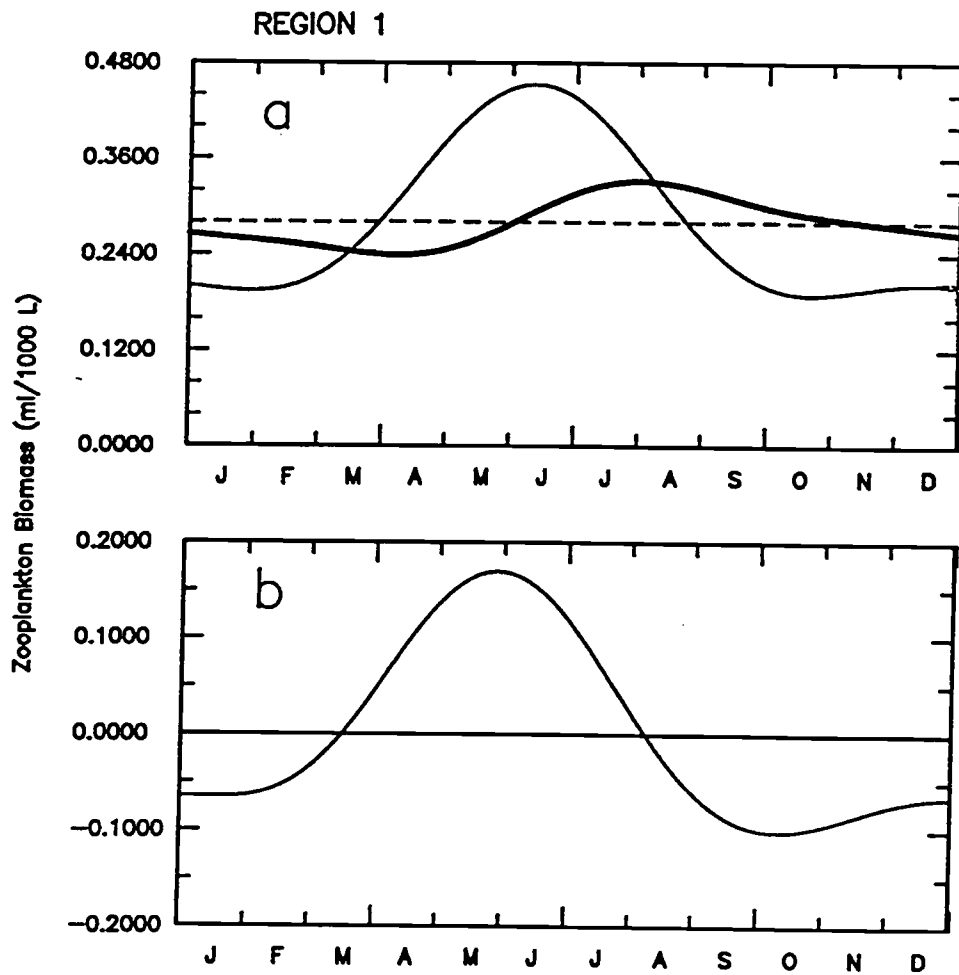


Figure 15 - For region 1, *a*, seasonal cycles of the volume integral of observed zooplankton biomass (solid line) and advected zooplankton biomass (thick solid line) in region 1. Also plotted is the seasonal mean of the observed zooplankton biomass as a dashed line
b, difference between the observed and advected zooplankton time series shown in panel *a*, representing the seasonal cycle of local zooplankton biomass.

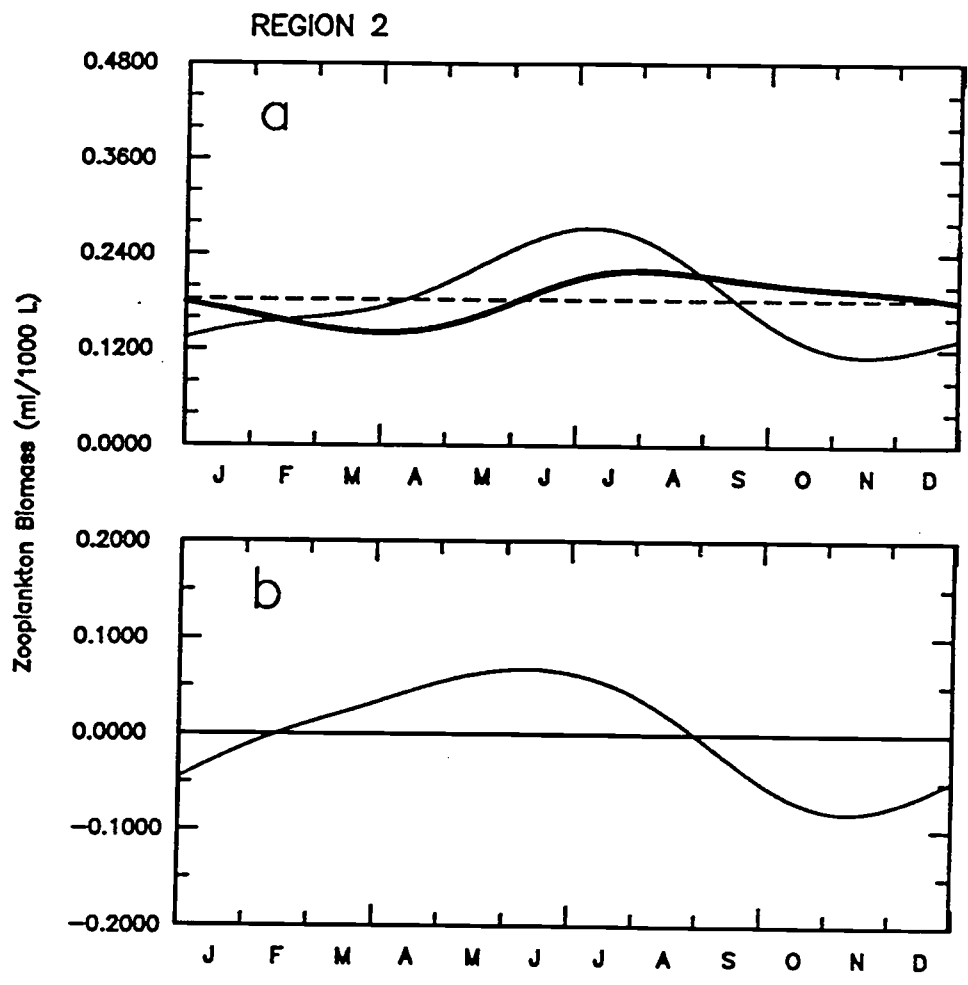


Figure 16 - Same as Figure 15, for region 2.

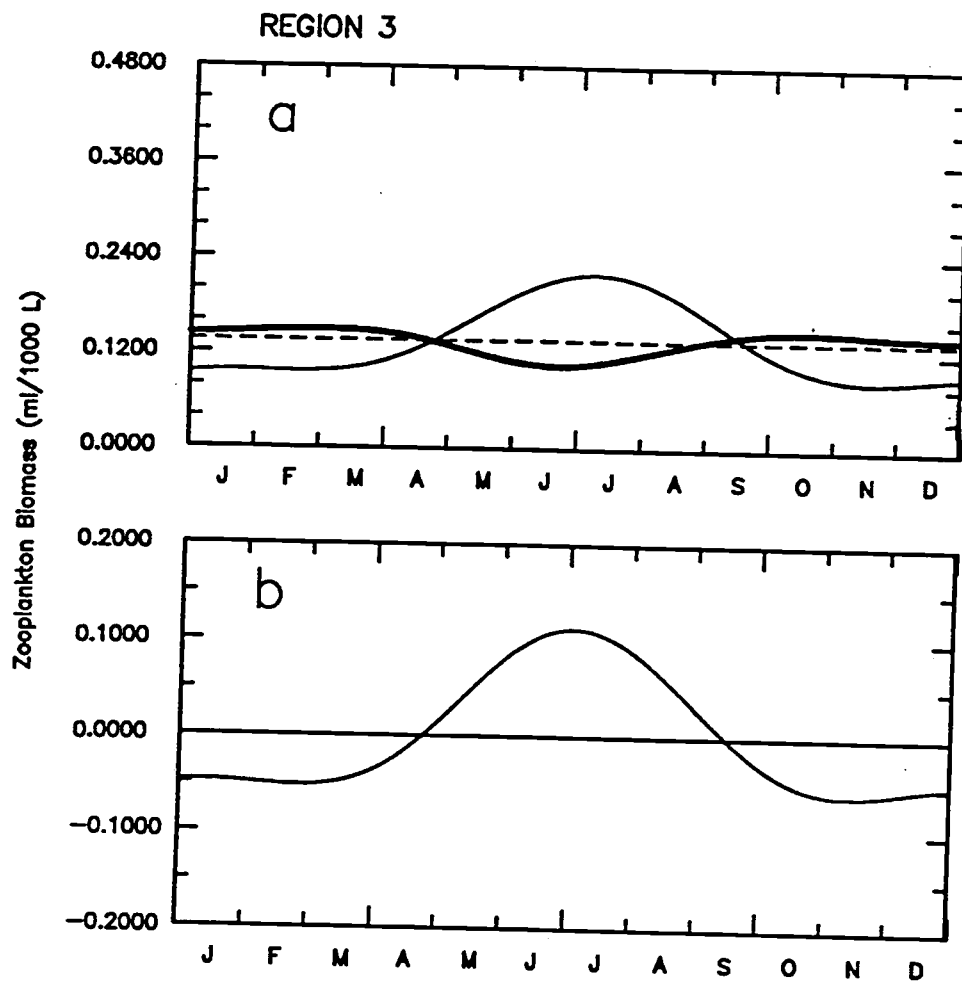


Figure 17 - Same as Figure 15, for region 3.

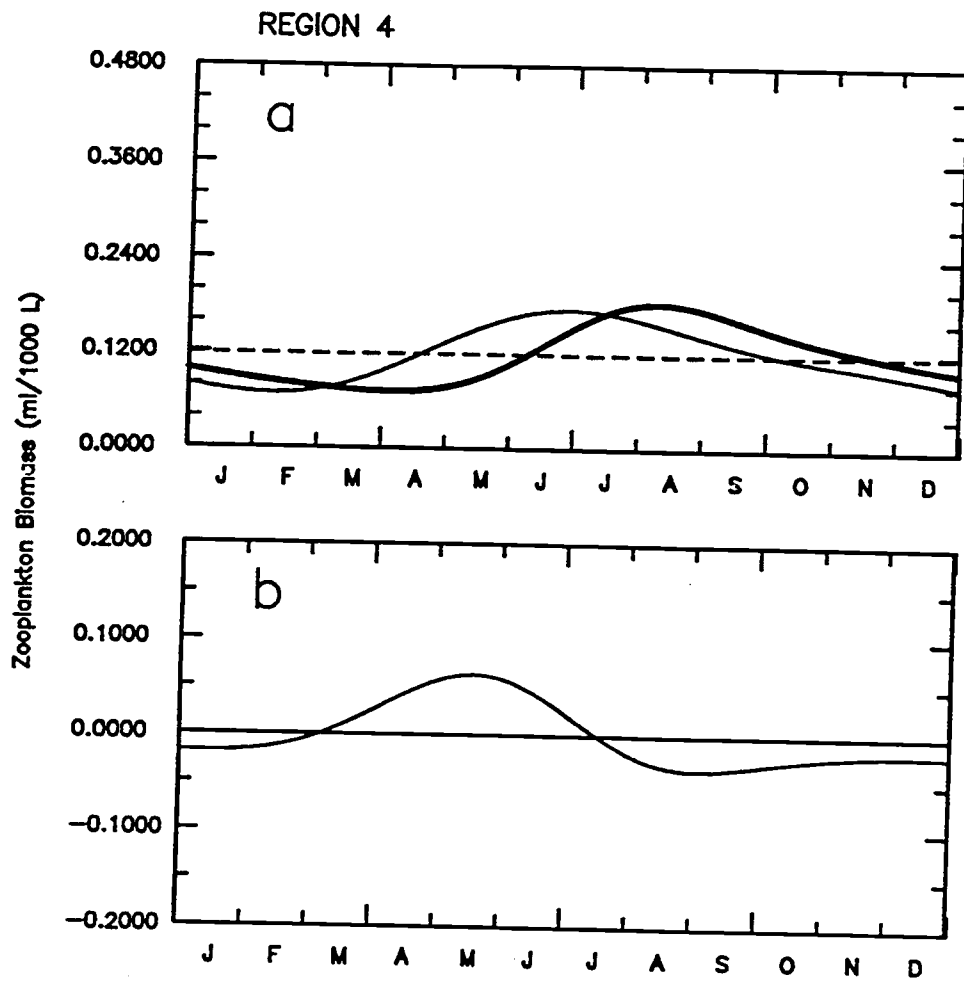


Figure 18 - Same as Figure 15, for region 4.

In region 3, the observed and advected components of zooplankton are roughly opposite in phase (Figure 17a). The maximum in the observed zooplankton occurring in summer is over two times the minimum value in the advected zooplankton. As a result, the maximum in the local component occurs at the same time as the maximum in the observed (Figure 17b).

DISCUSSION

The working hypothesis of the present study is that the observed pattern of seasonal zooplankton biomass is due to the passive advection of zooplankton populations by the California Current. The results of the model indicate that the seasonal large-scale advection does not fully explain the observed variability in zooplankton biomass. In each of the four regions studied, the seasonal patterns of the change in observed zooplankton biomass and NATZ are not equal in phase or amplitude over the seasonal cycle (Figures 10-13, panel d). These results contradict the conclusions of Roesler and Chelton (1987). Based on the co-occurrence of equatorward geostrophic velocity and zooplankton biomass maxima and minima, they concluded that the seasonal variability of large-scale zooplankton biomass is predominately controlled by alongshore transport of zooplankton throughout most of the California Current region, either through passive advection of zooplankton or local zooplankton response to advection of nutrients and/or phytoplankton.

In each of the four regions studied, the most significant transport of zooplankton is in the alongshore direction and is maximal in late spring to early summer (Figures 10-13, panel b). A gradient in the alongshore advection of zooplankton exists, with largest north to south advective fluxes in region 1 and smallest north to south fluxes in region 4. From Figures 6 and 8, both geostrophic and Ekman transports intensify in late spring and early summer and are fairly coincident over the entire study region. A separate calculation of alongshore advection of mass indicated that the transport is

relatively uniform over the study region with the peak southward advection occurring in late spring and early summer. These results indicate that an alongshore decrease in zooplankton abundance, rather than a decrease in mass transport, is the cause of the gradient in the alongshore transport of zooplankton.

Although the cross-shore transport of zooplankton biomass is small in comparison to the alongshore transport (see Figures 10-13, panel b), the magnitude of the cross-shore zooplankton divergence is similar to the magnitude of the alongshore zooplankton divergence in each of the four regions (Figures 10-13, panel c). This is due to a much larger cross-shore flux of zooplankton across the eastern boundary of each region because of strong east-west gradients of zooplankton arising from high zooplankton biomass near the coast, probably associated with coastal upwelling processes. These results indicate that the large-scale advection of zooplankton biomass is jointly dependent on both the alongshore and cross-shore transport components. Therefore, comparisons between the large-scale advection of zooplankton and the observed zooplankton biomass should include both alongshore and cross-shore transport components. In the study of seasonal zooplankton variability by Roesler and Chelton, cross-shore geostrophic velocities as well as Ekman transports were not considered.

Results from the box model clearly indicate that large-scale seasonal advection cannot fully explain the observed variability in zooplankton biomass. In each of the four regions studied, the seasonal patterns of the change in the CalCOFI zooplankton data and in NATZ are not equal in phase or amplitude over the seasonal cycle (Figures 10-13, panel d). Large advective

convergences, similar in magnitude to the observed changes in zooplankton, do occur in each of the four regions. However, a definite time lag exists between the change in the observed zooplankton and the modeled NATZ. The time lag ranges from less than one month in region 2 to over 3 months in region 3. It can be concluded that local sources and sinks of zooplankton and smaller scale advective events not resolved by the CalCOFI sampling pattern must be important in controlling the observed seasonal cycles of zooplankton biomass (Figures 14 and 15-18, panel b).

Small and mesoscale advective events clearly cannot be resolved from the model calculation of advection due to the spatial limitations of the data and the choice of region size. Furthermore, mesoscale advection events are highly undersampled in the CalCOFI data set as the sampling scheme is too infrequent and spatially patchy to resolve these processes. Any small or mesoscale advective event that acts to supply or remove zooplankton from each region should be included in the calculation of seasonal zooplankton biomass. Therefore, the estimates of local source/sink rates of zooplankton shown in Figure 14, as well as the estimates of zooplankton biomass due to local sources/sinks in Figures 15-18 panel b, likely include small and mesoscale advective zooplankton component. Due to the limitations in the CalCOFI data, the model results only resolve the large-scale seasonal variability of zooplankton biomass.

The influence of small to mesoscale processes on the large-scale seasonal cycle of zooplankton is not yet understood. Furthermore, as described above, only the large-scale patterns can be resolved in the CalCOFI zooplankton data. Therefore, the results of this model should be viewed only in

the context that the large-scale seasonal patterns of zooplankton biomass are not controlled by the large-scale advection of the California Current. Small and mesoscale advective processes as well as local growth patterns may have a greater influence in determining the seasonal patterns of zooplankton in the California Current ecosystem, and should be considered in future studies of seasonal zooplankton biomass distributions.

Are the rates of local growth/death obtained from this box model reasonable for each region? Unfortunately, general community estimates of local growth are required as the species composition of the CalCOFI zooplankton data is not known. Few studies have estimated secondary production rates of entire zooplankton communities. Even fewer studies have obtained even qualitative estimates of mortality rates. Huntley and Lopez (1992) have shown that temperature alone explains over 90% of the variance observed in marine copepod growth rates. Their work was based on an analysis of 181 separately published estimates of 33 species of marine copepod generation times in varying temperature ranges and varying biogeographical regions around the world. They determined the functional relationship between copepod growth rate (g in day^{-1}) and temperature (T in degrees Celsius) to be:

$$g = 0.0445 e^{0.111T}$$

with $r^2=0.91$. As estimates of sea surface temperature in the California Current can be obtained from the CalCOFI hydrographic data set, this relationship can be used to obtain a first-order estimate of the possible local growth rates in each region.

In order to compare the local growth rates obtained as a residual from the model to the values given by Huntley and Lopez, the maximum positive slope obtained in the estimate of local zooplankton abundance (Figures 15-18, panel b) during the spring was used to indicate the percentage of zooplankton growth per day. For each model region, a range of average sea surface temperatures observed during the spring months (from CalCOFI measurements) was chosen for the temperature parameter in the Huntley and Lopez growth model. The residual model calculation of local growth, as well as the temperature-dependent estimates of growth for each region, are shown in Table 2.

In all four regions, total zooplankton growth rates estimated from the box model and temperature agree to within a factor of 2-3, with particularly good agreement in region 3. In the northern-most region, the box model estimate of growth rate exceeds that of the Huntley and Lopez temperature-based estimate. This may be an indication that a portion of the local change in zooplankton in region 1 may actually be due to advection by small to mesoscale features such as filaments, which are not resolved by the model. This speculation is supported by the recent work by Smith and Lane (1991), who found that growth rates of 20 percent per day in *Eucalanus californicus* occurred in the core of a high biomass filament off the northern California coast. The surface temperature within the filament ranged from about 11-13° C during the sample period (Kosro et al., 1991). In these temperature ranges, a 15-18 percent growth rate is possible according to the temperature-based growth rate estimate given by Huntley and Lopez. Because these values are lower than the 20 percent growth rate observed by Smith and Lane, this

Table 2 - Estimates of local zooplankton growth rates. Temperature-based growth rates were calculated using Huntley and Lopez (1992) model of zooplankton growth. Sea surface temperature ranges were determined from CalCOFI measurements as the average temperatures observed in each region during spring. Model estimates of growth rates were obtained from Figures 15-18, panel b as the maximum positive slope.

	Spring sea surface temperature range (C)	Temperature-based growth rate (%/day)	Model growth rate estimate (%/day)
Region 1	13-14	19-21	27
Region 2	14-15	21-23	10
Region 3	15-16	23-26	18
Region 4	16-17	26-29	10

further implies that small to mesoscale advection as well as local growth likely occur in region 1.

In the other three regions, the temperature-based estimate of growth rate is greater than the box model estimate of local growth. This suggests that local growth of zooplankton is very small or parameter limited (i.e. food supply, predation), or due to small scale or mesoscale losses in these regions. Areas of strong coastal upwelling, such as regions 3 and 4, may be strongly affected by food limitation and therefore not as closely related to temperature.

The conclusion from these studies is that small scale or mesoscale features in the California Current may have a dramatic influence on the seasonal variability of zooplankton biomass. Off the coast of northern California, the above studies have shown that during the coastal upwelling season, significant offshore and alongshore transport of zooplankton biomass occurs on time scales shorter than one month. If the hypothesis of coastal filaments and jets acting as a seeding mechanism for certain dominant zooplankton species in offshore waters is true, then large amounts of local growth within the California Current are occurring. Further studies are needed in order to clearly determine effects of mesoscale zooplankton transport and production on the observed seasonal cycle. The CalCOFI sampling pattern (coarse spatial resolution and infrequent temporal sampling) is not adequate for these purposes.

SUMMARY

A simple box model was implemented to examine the effect of advection on the observed seasonal cycle of zooplankton in the California Current region. As with any model, the results should be interpreted in light of the various assumptions, and should not be considered as an exact representation of the California Current ecosystem. The limitations of the box model results are discussed in detail in Appendices A and B. However, the results of the present model are useful in that they provide a basis upon which future studies of the variability in seasonal zooplankton biomass distributions can be built. It is important to emphasize that this study only examines the seasonal variability zooplankton biomass. Different balances may be important to interannual variability. The general conclusions from this study are:

- 1.) Significant alongshore transport of zooplankton occurs during spring and summer with the largest transports of zooplankton biomass observed in the northern portion of the California Current.
- 2.) The large-scale advective transport is dependent on both the alongshore and cross-shore components (both geostrophic and Ekman) and acts to converge zooplankton biomass during the spring to summer season.
- 3.) Because the observed seasonal variability in the zooplankton distributions in the California Current leads to the advective flux of zooplankton by 1-3 months, the seasonal variability of zooplankton cannot be dominated by large-scale passive advective transport of zooplankton

populations, or nutrients from the northern regions. Assuming that the phase of seasonal variations in the advective flux of nutrients and/or phytoplankton is similar to that of the advective flux of zooplankton, advective transport of nutrients and/or phytoplankton, followed by local zooplankton growth, also cannot be the dominant mechanism controlling zooplankton variability in the California Current. This would require that the observed zooplankton productivity lag the advection, which contradicts the phase relationships found here.

4.) Other sources of variability must play an important role in determining the observed patterns of seasonal zooplankton abundance in the California Current region. Meso-scale processes, such as filament, jets and eddies, and local growth and loss in zooplankton biomass, which cannot be resolved in the CalCOFI data set, must be important sources of seasonal zooplankton variability in the California Current region.

REFERENCES

- Abbott, M.R. and B. Barksdale. 1991. Phytoplankton pigment patterns and wind forcing off central California. *J. Geophys. Res.*, 96: 14,649-14,667.
- Abbott, M.R. and P.M. Zion. 1985. Satellite observations of phytoplankton variability during an upwelling event. *Cont. Shelf Res.*, 4: 661-680.
- Bernal, P.A. 1981. A review of the low-frequency response of the pelagic ecosystem in the California Current. *Calif. Coop. Oceanic Fish. Invest. Rep.*, 22: 49-62.
- Bernal, P.A. and J.A. McGowan. 1981. Advection and upwelling in the California Current. In F.A. Richards (ed.), *Coastal upwelling*. American Geophysical Union, Washington, D.C. pp. 381-399.
- Bowman, T.E. and M.W. Johnson. 1973. Distributional atlas Calanoid copepods in the California Current region, 1949 and 1950. *Calif. Coop. Fish. Invest. Atlas 19*.
- Chavez, F.P., R.T. Barber, P.M. Kosro, A. Huyer, S.R. Ramp, T.P. Stanton, and B.R. De Mendiola. 1991. Horizontal transport and the distribution of Nutrients in the coastal transition zone off northern California: Effects on primary production, phytoplankton biomass and species composition. *J. Geophys. Res.*, 96: 14,833-14,848.
- Chelton, D.B. 1984. Seasonal variability of alongshore geostrophic velocity off central California. *J. Geophys. Res.*, 89: 3473-3486.
- Chelton, D.B. 1982. Large-scale response of the California Current to forcing by wind stress curl. *Calif. Coop. Fish. Invest. Rep.*, 23: 130-148.
- Chelton, D.B., P.A. Bernal, and J.A. McGowan. 1982. Large-scale interannual physical and biological interaction in the California Current. *J. Mar. Res.*, 40: 1095-1125.
- Coastal Transition Zone Group. 1988. The coastal transition zone program. *Eos Trans. AGU*, 69: 698-707.
- Colebrook, J.M. 1977. Annual fluctuations in biomass of taxonomic groups of zooplankton in the California Current, 1955-59. *Fish. Bull.*, 75: 357-368.
- Davis, R.E. 1985. Drifter observations of coastal surface currents during CODE: The method and descriptive view. *J. Geophys. Res.*, 90: 4,741-4,755.
- Fleminger, A. 1964. Distributional atlas of Calanoid copepods in the California Current region, part I. *Calif. Coop. Fish. Invest. Rep.*, 28: 59-96.

- Hemingway, G.T. 1979. A description of the California Current ecosystem by factor analysis. *Calif. Coop. Oceanic Fish. Invest. Atlas 2*.
- Hickey, B.M. 1979. The California Current system-hypothesis and facts. *Prog. Oceanogr.*, 8: 191-279.
- Hood, R.R., M.R. Abbott, A. Huyer and P.M. Kosro. 1990. Surface patterns in temperature, flow, phytoplankton biomass, and species composition in the coastal transition zone off northern California. *J. Geophys. Res.*, 95: 18,081-18,094.
- Huntley, M.E. and M.D.G. Lopez. 1992. Temperature-dependent production of marine copepods: A global synthesis. *Amer. Natural.*, 140: 201-242.
- Huyer, A. 1984. Hydrographic observations along the CODE Central Line off northern California. *J. Phys. Oceanogr.*, 14: 1,674-1,658.
- Huyer, A., P.M. Kosro, J. Fleischbein, S.R. Ramp, T. Stanton, L. Washburn, F.P. Chavez, T.J. Cowles, S.D. Pierce, and R.L. Smith. 1991. Currents and water masses of the Coastal Transition Zone off northern California, June to August 1988. *J. Geophys. Res.*, 96: 14,809-14,831.
- Kosro, P.M. and A. Huyer. 1986. CTD and velocity surveys of seaward jets off northern California. *J. Geophys. Res.*, 91: 7,680-7,690.
- Kosro, P.M., A. Huyer, S.R. Ramp, R.L. Smith, F.P. Chavez, T.J. Cowles, M.R. Abbott, P.T. Strub, R.T. Barber, P. Jessen, and L.F. Small. 1991. The structure of the transition zone between coastal waters and open ocean off northern California, winter and spring 1987. *J. Geophys. Res.*, 96: 14,707-14,730.
- Kundu, P.K. 1990. Fluid mechanics. Academic Press, Inc., New York.
- Large, P. and S. Pond. 1981. Open ocean momentum flux measurements in moderate to strong winds. *J. Phys. Oceanogr.*, 11: 324-326.
- Loeb, V.J., P.E. Smith and H.G. Moser. 1983. Ichthyoplankton and zooplankton abundance patterns in the California Current area, 1975. *Calif. Coop. Fish. Invest. Rep.*, 24: 109-131.
- Lynn, R.J. and J.J. Simpson. 1987. The California Current system: The seasonal variability of its physical characteristics. *J. Geophys. Res.*, 92: 12,947-12,966.
- Mackas, D.L., L. Washburn, and S.L. Smith. 1991. Zooplankton community pattern associated with a California Current cold filament. *J. Geophys. Res.*, 96: 14,781-14,797.
- Moum, J.N., D.R. Caldwell and P.J. Stabeno. 1988. Mixing and intrusions in a rotating cold-core feature off Cape Blanco, Oregon. *J. Phys. Oceanogr.*, 18: 823-833.

- NORPAC Committee. 1960. *Oceanic Observations of the Pacific, The NORPAC Atlas*. 11 pp., 123 plates. Univ. of Calif. Press, Berkeley.
- Pelaez, J. and J.A. McGowan. 1986. Phytoplankton pigment pattern in the California Current as determined by satellite. *Limnol. Oceanogr.*, 31: 927-950.
- Pond, S. and G.L. Pickard. 1983. *Introductory dynamical oceanography*. 2nd edition. Pergamon Press, New York.
- Raymont, J.E.G. 1980. *Plankton and productivity in the oceans, volume 1, phytoplankton*.
- Reid, J.L. 1962. On the circulation, phosphate-phosphorous content and zooplankton volumes in the upper part of the Pacific Ocean. *Limnol. Oceanogr.*, 7: 287-306.
- Reid, J.L. and R.A. Schwartzlose. 1962. Direct measurements of the Davidson Current off Central California. *J. Geophys. Res.*, 67: 2491-2497.
- Roemmich, D. 1989. Mean transport of mass, heat, salt and nutrients in southern California coastal waters: Implications for primary production and nutrient cycling. *Deep-Sea Res.*, 36: 1359-1378.
- Roesler, C.S. and D.B. Chelton. 1987. Zooplankton variability in the California Current, 1951-1982. *Calif. Coop. Fish. Invest. Rep.*, 28: 59-96.
- Ryther, J.H. 1969. Photosynthesis and fish production in the sea. *Science*, 166: 72-76.
- Simpson, J.J., T.D. Dickey, and C.J. Koblinsky. 1984. An offshore eddy in the California Current system, I, Interior dynamics. *Prog. Oceanogr.*, 13: 5-49.
- Smith, P.E. and R.W. Eppley. 1982. Primary production and the anchovy population in the Southern California Bight: comparison of time series. *Limnol. Oceanogr.*, 27: 1-17.
- Smith, S.L. and P.V. Lane. 1991. The jet off Point Arena, California: Its role in aspects of secondary production in the copepod *Eucalanus californicus* Johnson. *J. Geophys. Res.*, 96: 14,849-14,858.
- Strub, P.T., C. James, A.C. Thomas and M.R. Abbott. 1990. Seasonal and nonseasonal variability of satellite-derived surface pigment concentrations in the California Current. *J. Geophys. Res.*, 95: 11,501-11,530.
- Traganza, E.D., V.M. Silva, D.M. Austin, W.E. Hanson and S.H. Bronsink. 1983. Nutrient mapping and recurrence of coastal upwelling centers by satellite remote sensing: Its implication to primary production and the

- sediment record. In: Coastal upwelling: Its sediment record. Edited by E. Suess and J. Thiede, Plenum, New York.
- Walsh, J.J. 1977. A biological sketchbook for an eastern boundary current. In E.D. Goldberg, I.N. McCane, J.J. O'Brien, and J.H. Steele (eds.), *The sea*, volume 6, marine modeling. Wiley, New York. pp. 923-968.
- Washburn, L., D.C. Kadko, B.H. Jones, T. Hayward, P.M. Kosro, T.P. Stanton, S. Ramp and T. Cowles. 1991. Water mass subduction and the transport of phytoplankton in a coastal upwelling system. *J. Geophys. Res.*, 96: 14,927-14,946.

APPENDICES

APPENDIX A

Box Model Assumptions

One of the key assumptions made in this study is that vertical transport of zooplankton through the bottom of each region is negligible. This assumption can be tested by estimating the average vertical velocity at the bottom of each region (140 m). If the vertical velocity at the bottom of each region is identically zero, then the assumption of no vertical transport can be considered to be valid.

An estimate of the magnitude of the average vertical velocity in each region can be obtained using the continuity equation,

$$\frac{\partial w}{\partial z} = - \left[\frac{\partial u}{\partial x} + \frac{\partial v}{\partial y} \right]$$

The derivatives in the horizontal divergence on the right hand side of this equation can be approximated by taking horizontal velocity differences over a finite distance. Such finite differences are only applicable when the variations in horizontal velocities are smooth and nearly linear. As the dynamic height data were heavily smoothed after interpolation, the calculated horizontal velocity fields should be fairly smooth and well behaved. In areas of seasonally persistent meso-scale features, such as the geographically fixed Southern California Eddy, average vertical velocity estimates may be questionable as the horizontal velocities can vary greatly over small distances.

A first-order estimate of geostrophic vertical velocity, w_h , at depth h below the surface can then be made by integrating the horizontal divergence over a specified depth range.

$$w_0 - w_h = \int_{-h}^0 \frac{\partial w}{\partial z} dz = \int_{-h}^0 \left[\frac{\partial u}{\partial x} + \frac{\partial v}{\partial y} \right] dz$$

Since the vertical velocity vanishes at the sea surface (i.e. $w_0=0$), the vertical velocity at depth h is given by

$$w_h = -\int_{-h}^0 \left[\frac{\partial u}{\partial x} + \frac{\partial v}{\partial y} \right] dz \quad (1A)$$

In order for each box to remain in geostrophic mass balance, divergence in the vertical should likewise be zero, i.e., w_h should vanish. In each region, the geostrophic vertical velocity w_h was found to be six orders of magnitude smaller than the corresponding horizontal velocities throughout the year; fluctuations in the magnitude were random and averaged to zero over the seasonal cycle. The average geostrophic vertical velocity at the bottom of each region can thus be considered to be zero throughout the seasonal cycle. Therefore, the assumption of no geostrophic vertical transport of zooplankton can be considered to be a reasonable estimate.

The equation of continuity can also be used to estimate wind-driven vertical velocity. It has been previously shown that the integrated transport confined to the Ekman layer is equal to the wind stress divided by density times the Coriolis parameter (see Data Description and Methods section). The integrated Ekman mass transports can be represented as:

$$\rho \int_{-h}^0 u_{\text{Ekman}} dz = M_{\text{Ekman}}^x = \rho T_{\text{Ekman}}^x = \frac{\tau^y}{f}$$

$$\rho \int_{-h}^0 v_{\text{Ekman}} dz = M_{\text{Ekman}}^y = \rho T_{\text{Ekman}}^y = -\frac{\tau^x}{f}$$

The wind driven vertical velocity (denoted as w_{Ekman}) can be derived in a manner similar to the geostrophic vertical velocity by multiplying the equation of continuity by density and integrating from some depth $z=-D$ to the surface. Note that in the following derivations, the depth of integration is denoted as D , and represents the depth of the Ekman layer.

$$\rho \int_{-D}^0 \frac{\partial w}{\partial z} dz = \rho \int_{-D}^0 \left[\frac{\partial u}{\partial x} + \frac{\partial v}{\partial y} \right] dz$$

$$-\rho [w_{\text{Ekman}}(0) - w_{\text{Ekman}}(-D)] = \frac{\partial}{\partial x} \int_{-D}^0 \rho u dz + \frac{\partial}{\partial y} \int_{-D}^0 \rho v dz$$

Since the vertical velocity vanishes at the sea surface, this equation reduces to

$$\rho w_{\text{Ekman}}(-D) = \frac{\partial}{\partial x} M_{\text{Ekman}}^x + \frac{\partial}{\partial y} M_{\text{Ekman}}^y = \frac{\partial}{\partial x} \left(\frac{\tau^y}{f} \right) + \frac{\partial}{\partial y} \left(-\frac{\tau^x}{f} \right)$$

Solving for the vertical velocity at depth $z=-D$:

$$w_{\text{Ekman}}(-D) = \frac{1}{\rho f} \left[\frac{\partial \tau^y}{\partial x} - \frac{\partial \tau^x}{\partial y} \right] + \frac{\beta}{f^2} \tau^x$$

In this representation, the vertical velocity at depth $z=-D$ is equal to the wind stress curl divided by density times the Coriolis parameter plus a Beta term. The Beta term arises from differentiating $1/f$ in the north/south direction. The Beta term can be ignored since it is small in comparison to the wind stress curl. The vertical velocity at depth $z=-D$ is then approximately equal to the horizontal Ekman transport divergence.

$$\rho w_{\text{Ekman}}(-D) \equiv \frac{\partial}{\partial x} M_{\text{Ekman}}^x + \frac{\partial}{\partial y} M_{\text{Ekman}}^y = \frac{\partial}{\partial x} \left(\frac{\tau^y}{f} \right) + \frac{\partial}{\partial y} \left(-\frac{\tau^x}{f} \right) \quad (2A)$$

The vertical velocity is calculated in this fashion here because the Ekman transports were also used in the calculation of advective transport.

Note that the actual depth at which the wind driven vertical velocity is estimated is unknown. This unknown depth is considered to be at the base of the layer of the ocean influenced by wind forcing, more commonly known as the Ekman layer. Typically, the Ekman layer is thought to be contained in the upper 100 m of the ocean. In a study of vertical mixing along fronts in the coastal jet off Point Arena, California, Dewey and Moum (1990) found that the wind mixed layer consistently resides in the upper 100 m. The time series of average vertical velocity in each region, calculated from the divergence of the horizontal Ekman transport are shown in Figure 19. A negative value indicates a downwelling velocity, while a positive value denotes an upward velocity or Ekman pumping.

The maximum magnitude wind-driven vertical velocity calculated from equation 2A is on the order of 10^{-4} mm per second. Even if the base of the Ekman layer was located near or below the bottom of each region (140 m) it is unlikely that significant zooplankton biomass would be transported by this velocity, as most zooplankton captured by the vertical net tows can swim faster than 10^{-2} mm per second. Therefore, as with geostrophic vertical velocity, the vertical transport of zooplankton by wind-driven currents can be considered to be negligible.

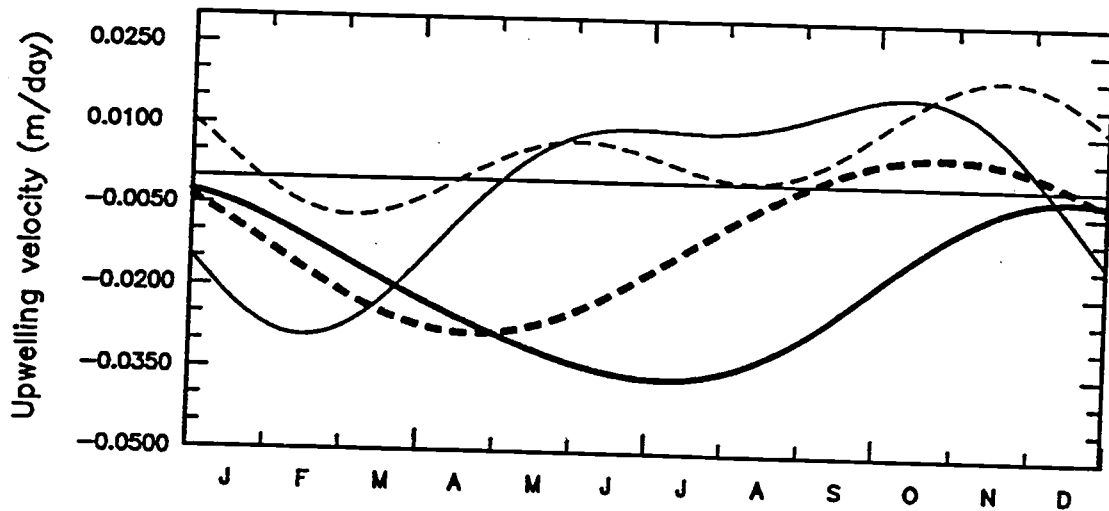


Figure 19 - Seasonal cycles of wind-driven upwelling velocity averaged over each of the four regions. Region 1 is plotted as a solid line, region 2 as a dashed line, region 3 as a thick solid line and region 4 as a thick dashed line.

Another key assumption made in this study is that the vertical profile of horizontal geostrophic velocity is constant from the sea surface to 140 meters. While not essential, this simple model for the vertical structure of horizontal velocity greatly simplifies the calculations in the box model. However, large vertical variations in alongshore geostrophic velocity occur in the core of the California Current and the Inshore Countercurrent (Chelton, 1984; Lynn and Simpson, 1987). The difference between the surface and 200 m alongshore geostrophic velocity can be as great as 16 cm s^{-1} during the spring in the core of the California Current. Clearly, the assumption of constant geostrophic velocity, equal to the surface value, is not valid.

The horizontal transport of zooplankton is jointly dependent on the vertical profiles of velocity and zooplankton. As with the horizontal velocity, a constant vertical structure of zooplankton from 0 to 140 m was used in the model. A clear understanding of the seasonal vertical distributions of zooplankton biomass offshore of the continental slope has not yet been determined. Thus, it is difficult to estimate the reliability of a constant vertical profile of zooplankton in representing the real ocean. While changing the vertical profile of zooplankton biomass would alter the amplitude of the NATZ, the phase however, would probably not change significantly. Only by allowing the vertical profile of zooplankton to vary over the seasonal cycle could the phase of the NATZ be altered. This is more likely to be the case in the open ocean due to zooplankton ontogenetic migrations. Until a better understanding of the seasonal zooplankton biomass vertical distributions in the offshore regions is attained, further alterations of the constant vertical profile used in the model would be based on conjecture. Thus, for the time

being, the assumption of a constant vertical distribution of zooplankton biomass can be taken as a reasonable first-order estimate.

It should be noted that the box model calculations in this study all involve vertical integrals over the upper 140 meters. The next order model for the vertical structure would therefore be to replace the surface values used here with a simple linear profile that decreases to a value of zero at a depth of 140 meters. The results for this model could then be compared with those obtained by this study for a constant vertical profile to determine the sensitivity of the results to vertical structure.

APPENDIX B

Interpolations of Zooplankton and Dynamic Height Data

In order to estimate the reliability of the interpolation methods used (see Data Description and Methods) to estimate the seasonal distributions of zooplankton and dynamic height, a simple test was performed using analytical data. Analytical fields of spatially periodic data at varying wavelengths were formed over the fine mesh grid. Using the analytical data at only the raw data sample points (zooplankton and dynamic height), separate interpolations of the data were performed. In each region, the interpolated values were compared with the analytical values at each grid point within the region. The average root mean square (rms) difference was calculated for each wavelength tested.

Figure 20 shows the rms error obtained from interpolations onto the 10 km grid constructed from the analytical data at the 14 zooplankton areal averaged data locations. Generally, the interpolated zooplankton values are least reliable at short wavelengths (<300 km), as indicated by rms errors greater than 0.5. Interpolations of longer wavelength features (>300 km) are only slightly more reliable. In regions 2 and 3, increases in the rms errors are observed at 400 km. However, both regions reach their lowest values at 500 km. The results of this analysis indicate that the interpolation method used for the zooplankton data may only be reliable at representing the very large-scale features observed in each region. This is because the zooplankton areal averaged data locations are widely spaced.

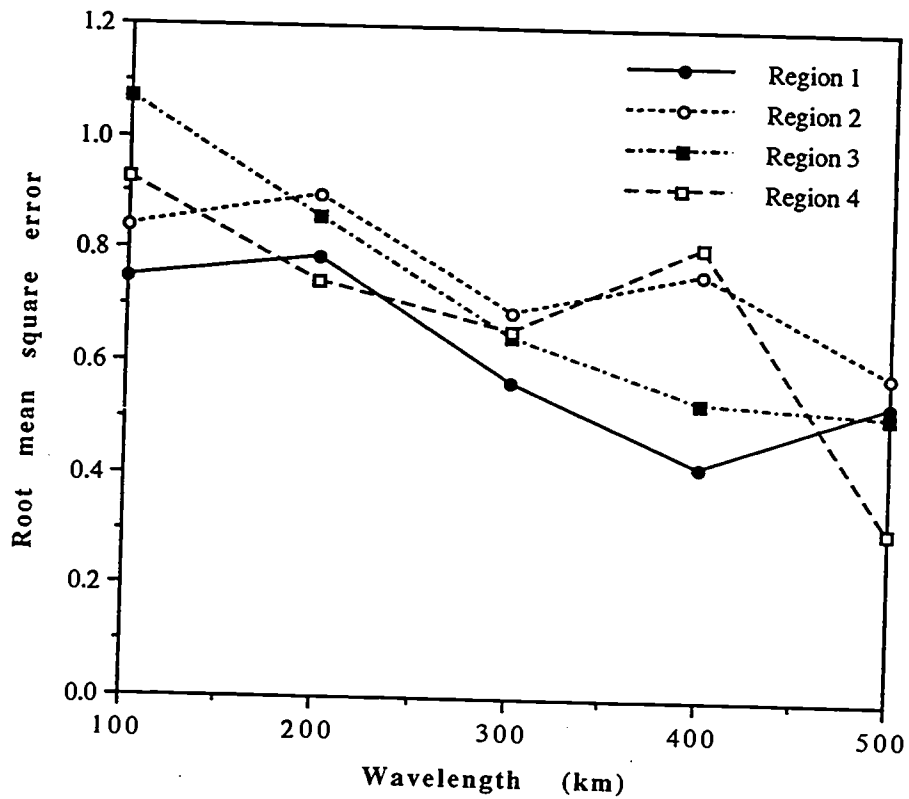


Figure 20 - Root mean square error obtained from interpolations of varying wavelength analytical data using the 14 zooplankton grid point locations used in this study.

The rms errors of the interpolations of the analytical data using the 149 dynamic height grid points from this study are shown in Figure 21. An exponential decrease in rms error with increasing wavelength is observed in regions 2, 3 and 4. In these three regions, the rms error is less than 0.3 at 300 km and decreases to about 0.1 at 500 km. The decrease in the rms error in region 1 is approximately linear, reaching a value of less than 0.2 at 500 km. The slower decrease in rms error in region 1 than in the other three regions is because region 1 contains the fewest dynamic height data points (see Figure 4). These results indicate that the interpolation method used for the dynamic height data is very reliable at representing long wavelength features and even resolves some of the larger mesoscale features.

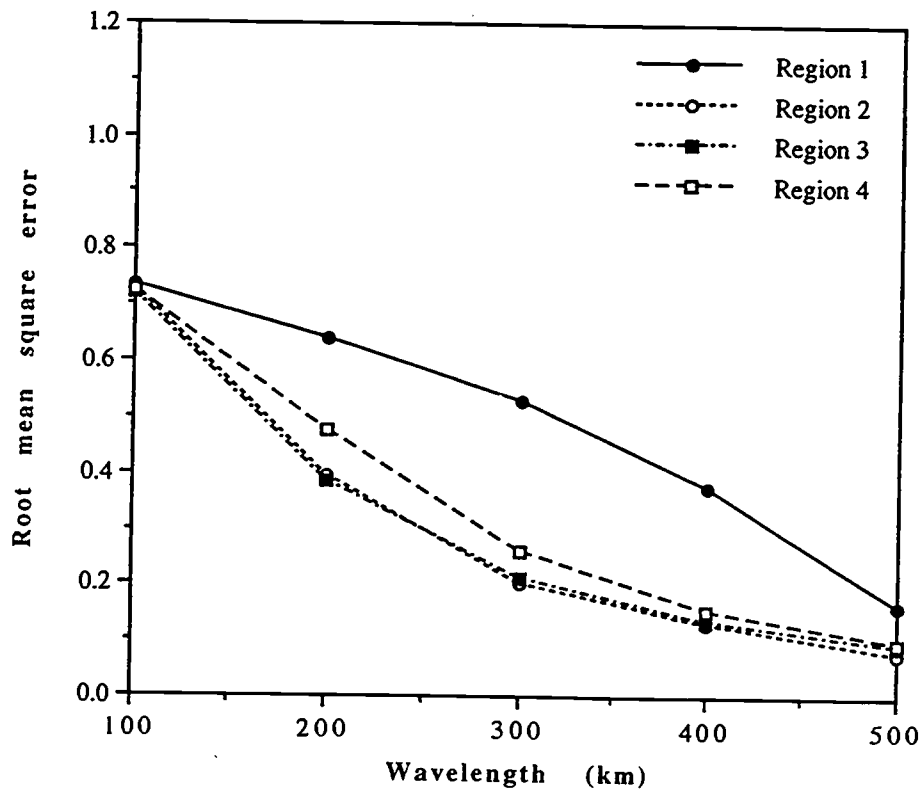


Figure 21 - Same as Figure 20, using the 149 dynamic height grid point locations.

APPENDIX C

The Appearance and Removal of Secular Terms

As described in the Methods Section, the time series of the NATZ was calculated by taking the line integral of observed zooplankton biomass times transport (geostrophic and Ekman) at each grid point along the boundary of each region (see Data Description and Methods section, equation 7). Recall that the time series of zooplankton biomass and transport are estimated by least squares regression onto an annual and semiannual seasonal cycle, and thus consist of 4 harmonic terms plus a constant offset. The time series of advected zooplankton biomass was estimated by integrating the NATZ over the seasonal cycle.

In Figures 10-14, panel d, it is clear that seasonal mean of the NATZ is not identically zero (i.e., the constant offset terms in the regressions are nonzero). A nonseasonal mean in the NATZ would imply a secular component of increase or decrease (depending on the sign) in the advected zooplankton biomass computed from the time integral of the NATZ. Over the seasonal cycle, this secular increase/decrease must be balanced by local processes occurring within each region since a secular increase in zooplankton biomass is nonbiological. This secular component must therefore be removed from the time series of advected zooplankton.

Showing the exact derivation of all secular terms produced in the time integral of the NATZ is straightforward but long and tedious, as over one hundred multiplications of zooplankton times transport were performed at

each time step. For the ease of discussion, the following example is given to show why the secular terms appear and how they are removed from advected zooplankton time series. In this example, the time series of observed zooplankton biomass and transport contain only one harmonic term and a constant offset. The line integration step has been omitted by assuming that the time series of zooplankton biomass and transport have been integrated over a small volume. Therefore, the multiplication of these two time series should indicate the advection of zooplankton biomass through this small volume.

Consider two time series, A and B, each consisting of a single harmonic term with angular frequency ω plus a constant. In this example, take A to represent the time series of observed zooplankton biomass, and B to represent the time series of transport integrated over a small volume,

$$A(t) = a_0 + a_1 \sin(\omega t)$$

$$B(t) = b_0 + b_1 \sin(\omega t)$$

The time series of the advection of zooplankton, denoted as C' , can be calculated by multiplying A and B,

$$C'(t) = A(t) * B(t) = a_0 b_0 + (a_0 b_1 + a_1 b_0) \sin(\omega t) + a_1 b_1 \sin^2(\omega t)$$

By setting

$$c_0 = a_0 b_0$$

$$c_1 = a_0 b_1 + a_1 b_0$$

$$c_2 = a_1 b_1$$

then,

$$C'(t) = c_0 + c_1 \sin(\omega t) + c_2 \sin^2(\omega t). \quad (1C)$$

This time series represents the change in seasonal zooplankton due to advection through this small volume.

The time series of zooplankton biomass due to advection can be estimated by integrating equation 1C over time,

$$C(t) = \int C'(t) dt = c_0 t - \frac{c_1}{\omega} \cos(\omega t) + \frac{c_2}{2} t - \frac{c_2}{4\omega} \sin(2\omega t) + c_3 \quad (2C)$$

This time integration thus produces the secular terms, $c_0 t$ and $\frac{c_2}{2} t$. In this simple example, the removal of these secular terms can be easily done by excluding them in the time integration. However, as mentioned above, in the model used in this study, the regressions of the data consist of three additional harmonic terms. Furthermore, the removal of these secular terms produced by the multiplication of zooplankton times geostrophic and Ekman transports would have to be performed at each individual grid point along the boundary of each region. Clearly this would be a time consuming task. However, it can be shown that all secular terms can be removed by making a simple linear adjustment of the advected zooplankton time series.

Returning to the above example, equation 1C is now integrated over the seasonal cycle, $t=0$ to $t=T$,

$$\int_0^T C'(t) dt = C(T) - C(0) = \left[c_0 \cdot T + c_1 \int_0^T \sin(\omega t) dt + \frac{c_2}{2} \cdot T + c_2 \int_0^T \sin(2\omega t) dt + c_3 \right] \\ - \left[c_0 \cdot 0 + c_1 \int_0^0 \sin(\omega t) dt + \frac{c_2}{2} \cdot 0 + c_2 \int_0^0 \sin(2\omega t) dt + c_3 \right]$$

The integrals of the harmonic terms equate to zero over a period. Solving for the coefficients of the secular terms shown in 2C,

$$c_0 + \frac{c_2}{2} = \frac{C(T) - C(0)}{T}$$

Therefore, the sum of the coefficients of all secular terms can be solved for by taking the difference in advected zooplankton at the start and end of the seasonal cycle and dividing by the period. Having solved for all the secular terms in this manner, a simple linear adjustment can be applied to form the seasonal time series of advected zooplankton.